MARMARA UNIVERSITY

INSTITUTE FOR GRADUATE STUDIES IN PURE AND APPLIED SCIENCES

INVESTIGATION OF POLYMORPHIC PHASE TRANSFORMATION OF CALCIUM CARBONATE IN THE PRESENCE OF DIFFERENT ADDITIVES

TUBA NUR ÖZALP-ŞENDUR

MASTER THESIS

Department of Chemical Engineering

Thesis Supervisor
Prof. Dr. Perviz SAYAN

Thesis CO- Supervisor
Assoc. Prof. Dr. Sevgi POLAT

ISTANBUL, 2021

MARMARA UNIVERSITY

INSTITUTE FOR GRADUATE STUDIES IN PURE AND APPLIED SCIENCES

INVESTIGATION OF POLYMORPHIC PHASE TRANSFORMATION OF CALCIUM CARBONATE IN THE PRESENCE OF DIFFERENT ADDITIVES

TUBA NUR ÖZALP-ŞENDUR

524518002

MASTER THESIS

Department of Chemical Engineering

Thesis Supervisor
Prof. Dr. Perviz SAYAN

Thesis CO- Supervisor
Assoc. Prof. Dr. Sevgi POLAT

ISTANBUL, 2021

ACKNOWLEDGEMENTS

To start, I would like to express my sincere gratitude to my esteemed supervisor, Prof. Dr. Perviz SAYAN, who shared his knowledge and experience with me, guided me to the study with his ideas, opinions, and suggestions.

I would like to thank my co-supervisor, Assoc. Prof. Dr. Sevgi POLAT, for her patience, advice, understanding, guidance, and knowledge to assist me during my thesis. Although we were having a complex time because of COVID-19, she was always encouraging and motivating me.

This work was supported by Marmara University Scientific Research Projects Commission (BAPKO) under the funding FYL-2020-10025.

Finally, I would like to thank my family and my dear husband for their trust, eternal love and support me during this project and every stage of my life.

06/2021 **Tuba Nur ÖZALP-ŞENDUR**

CONTENTS

ACKNOWLEDGEMENTS **1**

CONTENTS ..... **ii**

ABSTRACT ..... **vi**

SYMBOLS ..... **vii**

ABBREVATIONS ..... **viii**

LIST OF FIGURES ..... **viii**

LIST OF TABLES ..... **xii**

1. INTRODUCTION **1**

1.1. The Purpose of the Study 1

1.2. Calcium Carbonate, Polymorphs and Properties 2

1.3. Polymorphism 4

1.4. Crystallization 5

1.4.1. Supersaturation 6

1.4.2. Nucleation 7

1.4.3. Crystal Growth 8

1.5. Effects of Additives/Impurities on Pollymorphism and Crystallization 9

1.6. Amino Acids 10

1.6.1. Tryptophan 14

1.6.2. Glutamic Acid 14

1.6.3. Threonine 15

1.7. Studies About Calcium Carbonate Polymorphism 15

1.8. Characterization Techniques 19

1.8.1. X-ray Diffraction Analysis (XRD) 19

1.8.2. Fouirer Transform Infrared Spektrofotometer (FTIR) 21

1.8.3. Scanning Electron Microscopy (SEM) 21
1.8.4. Atomic Force Microscopy (AFM) 22
1.8.5. Zeta Potential 24
1.8.6. Thermogravimetric Analysis (TGA) 25
2. MATERIALS AND METHOD 28
2.1. Materials 28
2.2. Experimental Method 28
2.3. Analysis 29
3. RESULTS AND DISCUSSION 30
3.1. The Results of Effects of Tryptophan on the Polymorphic Transformation of Calcium Carbonate. 30
3.1.1. XRD Analysis. 30
3.1.2. FTIR Analysis. 32
3.1.3. SEM and AFM Analysis. 33
3.1.4. Zeta Potential Analysis. 38
3.1.5. Filtration Analysis. 39
3.1.6. Thermogravimetric Analysis. 40
3.1.7. Kinetic and Thermodynamic Analysis 42
3.1.8. Experiment Design Results 45
3.2. The Results of Effects of Glutamic Acid on the Polymorphic Transformation of Calcium Carbonate. 50
3.2.1. XRD Analysis. 50
3.2.2. FTIR Analysis. 50
3.2.3. SEM Analysis. 53
3.2.4. Zeta Potential Analysis. 57
3.2.5. Filtration Analysis. 57

3.3. The Results of Effects of Threonine on the Polymorphic Transformation of Calcium Carbonate. 59

3.3.1. XRD Analysis. 59

3.3.2. FTIR Analysis. 59

3.3.3. SEM Analysis. 62

3.3.4. Zeta Potential Analysis. 65

3.3.5. Filtration Analysis. 65

4. CONCLUSIONS 67

REFERENCES 69

LIST OF PUBLICATIONS ABOUT THE THESIS SUBJECT BEING PREPARED 79

ÖZET

KALSİYUM KARBONATIN POLİMORFİK FAZ DÖNÜŞÜMÜNÜN ÇEŞİTLİ KATKILAR VARLIĞINDA İNCELENMESİ

Kalsiyum karbonat ($CaCO_3$) kristalleri, katkı maddesi olarak seçilen triptofan, glutamik asit ve treonin varlığında 30 °C sıcaklık ve pH 8.5'da üretilmiştir. Bu tez çalışması kapsamında (i) triptofan, glutamik asit ve treonin katkı maddelerinin $CaCO_3$'ın polimorfik faz dönüşümü üzerindeki etkilerini belirlemek, (ii) Coats-Redfern modeli kullanarak kinetik ve termodinamik açısından saf $CaCO_3$'ın termal bozunma özelliklerini araştırmak ve (iii) yanıt yüzey yöntemi ile deneysel koşulların $CaCO_3$ kristallerinin vaterit polimorfu üzerindeki etkisini incelemek amaçlanmıştır. İlk olarak, $CaCO_3$ kristalleri üretilmiş ve bu kristallerin XRD, FTIR, SEM, BET, AFM ve zeta potansiyel analizleri yapılmıştır. Elde edilen bu sonuçlara göre, $CaCO_3$ kristallerinin şekilleri pürüzsüz kübik kalsit kristallerinden artan triptofan, glutamik asit ve treonin konsantrasyonları ile gözenekli düzensiz küresel formlu vaterit kristallerine dönüşmüştür. XRD ve FTIR analiz sonuçları, kullanılan her üç katkı maddesi için t=30 dak. ve 50 ppm konsantrasyonunda hem kalsit hem de vaterit polimorfunun birlikte oluştuğunu göstermiştir. Katkı maddelerinin konsantrasyonunun artırılmasıyla sadece vaterit formunda $CaCO_3$ kristalleri elde edilmiştir. Zeta potansiyeli analiz sonuçları, yüksek glutamik asit konsantrasyonunun kristallerin yüzey yüklerinin pozitif, düşük konsantrasyonlarda ise negatif elektrik yüküne sahip kristaller olduğunu göstermiştir. Filtrasyon analiz sonuçlarına göre kullanılan tüm katkı maddelerinin saf ortama kıyasla daha az spesifik bir kek direnci değerine sahiptir. Kinetik analiz sonuçları, $CaCO_3$'ın termal bozunma sürecinin R_3 mekanizması ile uyumlu olduğunu göstermiştir. Kristallerin termal bozunması sırasında ortalama aktivasyon enerji değeri 224.6 kJ/mol olarak hesaplanmıştır. Deney tasarım sonuçlarına göre, triptofan konsantrasyonun üretilen kristallerdeki vaterit polimorf miktarını etkileyen değişkendir. Sonuç olarak, bu çalışma farklı katkı maddeleri varlığında $CaCO_3$ kristallerinin polimorfunu, boyutunu ve morfolojisini daha iyi anlamak ve kontrol etmek için önemli sonuçlar içermektedir.

Anahtar kelimeler: Kalsiyum karbonat; polimorfizm; merkez esaslı kompozit dizayn; kristal morfolojisi; katkı maddesi; kinetik; termodinamik.

ABSTRACT

INVESTIGATION OF POLYMORPHIC PHASE TRANSFORMATION OF CALCIUM CARBONATE IN THE PRESENCE OF DIFFERENT ADDITIVES

The calcium carbonate ($CaCO_3$) crystals were successfully synthesized in the presence of tryptophan, glutamic acid, and threonine used as the additives at 30 °C and at a pH of 8.5. The objectives of this study were to: (i) determine the effects of tryptophan, glutamic acid, and threonine on the polymorphic phase transformation of $CaCO_3$, (ii) investigate the thermal degradation characteristics of $CaCO_3$ in terms of kinetics and thermodynamics using the Coats–Redfern method, and (iii) assess the influence of the experimental conditions on the vaterite composition of $CaCO_3$ using response surface methodology based on central composite design. First, the $CaCO_3$ crystals were prepared and analyzed using XRD, FTIR, SEM, BET, AFM, and zeta potential analysis. Based on the characterization results, the shape of the $CaCO_3$ crystals changed from smooth cubic calcite crystals to porous irregular spherical-like vaterite crystals with increasing tryptophan, glutamic acid, and threonine concentrations. XRD and FTIR results showed that that both calcite and vaterite in forms of apparently $CaCO_3$ crystals were obtained in the presence of 50 ppm all additive concentration at t=30 min. When increasing all additive concentrations in the suspension, the formed $CaCO_3$ were only in the vaterite form. Zeta potential analysis indicated that higher additive concentration resulted in a positive surface charge of the crystals, whereas lower concentration gave negative electrical charge for glutamic acid media. Filtration analysis pointed out that adding all additives resulted in a less specific cake resistance value than that in pure media. Meanwhile, the kinetic results illustrated that the thermal degradation of $CaCO_3$ followed the shrinkage geometrical spherical mechanism, R_3 and the average activation energy was 224.6 kJ/mol. According to the results of the experimental design, the tryptophan concentration was the most influential variable affecting the relative fraction of vaterite in the produced crystals. It can be concluded that tryptophan, glutamic acid, and threonine are important for better understanding and controlling the polymorph, size, and morphology of $CaCO_3$ crystals.

Keywords. Calcium carbonate; polymorphism; central composite design; crystal morphology; additive; kinetics; thermodynamics.

SYMBOLS

A **:** Pre-exponential factor (min^{-1})

E **:** Activation energy (kJ/mol)

f(x) **:** Reaction model

g(x) **:** Integrated form of the reaction model

k(T) **:** Reaction rate constant

n : Reaction order

R **:** Ideal gas constant (8.314 J/mol.K)

T **:** Absolute temperature (K)

x **:** Conversion

β : Heating rate (°C/min)

ΔG° : Gibbs free energy change (kJ/mol)

ΔH° : Standard enthalpy change (kJ/mol)

ΔS° : Standard entropy change (J/mol.K)

ABBREVATIONS

AFM	**:** Atomic force microscopy
BET	**:** Brunauer-Emmett-Teller
$CaCO_3$	**:** Calcium carbonate
DTG	**:** Differential thermogravimetric
EPR	**:** Electron paramagnetic resonance
FTIR	**:** Fourier transform infrared
RSM	**:** Response surface methodology
CCD	**:** Central composite design
SEM	**:** Scanning electron microscopy
TEM	**:** Transmission electron microscopy
TGA	**:** Thermogravimetric analysis
XRD	**:** X-ray diffraction

LIST OF FIGURES

Figure 1.1. Polymorphs of calcium carbonate 3

Figure 1.2. SEM images of the calcium carbonate polymorphs a) calcite, b) vaterite and c) aragonite 3

Figure 1.3. Schematic illustration of polymorphs and hydrate.....4

Figure 1.4. Solubility curves in case of polymorphy.....5

Figure 1.5. Solubility-supersaturation curve 7

Figure 1.6. Nucleation mechanism 8

Figure 1.7. The structure of amino acid.....10

Figure 1.8. Molecular structure of tryptophan.....14

Figure 1.9. Molecular structure of glutamic acid 14

Figure 1.10. Molecular structure of threonine 15

Figure 1.11. Schematic representation of reflections from adjacent planes within the crystal 19

Figure 1.12. Diagram of a simple X-ray diffraction.....20

Figure 1.13. X-Ray tube 20

Figure 1.14. Schematic representation of Fourier transform infrared spectroscopy 21

Figure 1.15. The representation of SEM 22

Figure 1.16. Schematic representation of atomic force microscope.....23

Figure 1.17. Images obtained by atomic force microscope 24

Figure 1.18. Visualization for electrical double layer of a particle suspended in a liquid. 25

Figure 1.19. Schematic representation of thermogravimetric analysis.....26

Figure 2.1. The experimental setup. 28

Figure 3.1. XRD results for $CaCO_3$ crystals precipitated in pure media and media supplemented with 50 and 100 ppm tryptophan. 31

Figure 3.2. FTIR results for $CaCO_3$ crystals precipitated in pure media and media supplemented with 50 and 100 ppm tryptophan. 32

Figure 3.3. SEM images of $CaCO_3$ crystals precipitated in pure media.....34

Figure 3.4. EDX results of $CaCO_3$ crystals precipitated in pure media. 34

Figure 3.5. SEM images for $CaCO_3$ crystals precipitated with 50 ppm tryptophan at t = 30 min (a) and at t = 100 min (b). 35

Figure 3.6. SEM images for $CaCO_3$ crystals precipitated with 100 ppm tryptophan at t = 30 min (a) and at t = 100 min (b). 36

Figure 3.7. 3D micrographs for the crystals precipitated without (a) and with 100 ppm tryptophan (b). 38

Figure 3.8. The change of zeta potential with time for tryptophan media.....39

Figure 3.9. TG and DTG curves of $CaCO_3$ crystals precipitated in pure media. 41

Figure 3.10. TG and DTG curves of $CaCO_3$ crystals precipitated with 100 ppm tryptophan 41

Figure 3.11. 3D-surface and contour plots showing the effects of (a) temperature and stirring rate; (b) temperature and tryptophan concentration; and (c) stirring rate and tryptophan concentration on the vaterite composition. 49

Figure 3.12. XRD results for $CaCO_3$ crystals precipitated in pure media and media supplemented with 50 and 100 ppm glutamic acid.....51

Figure 3.13. FTIR results for $CaCO_3$ crystals precipitated in pure media and media supplemented with 50 and 100 ppm glutamic acid.....52

Figure 3.14. SEM images for $CaCO_3$ crystals acquired media supplemented with 50 ppm glutamic acid at t = 30 min (a) and at t = 100 min (b). 54

Figure 3.15. SEM images for $CaCO_3$ crystals acquired media supplemented with 100 ppm glutamic acid at t = 30 min (a) and at t = 100 min (b). 55

Figure 3.16. Particle size distributions for $CaCO_3$ crystals acquired in pure media (a) and media supplemented with 50 ppm glutamic acid (b) and with 100 ppm glutamic acid (c). 56

Figure 3.17. The change of zeta potential with time for glutamic acid media 57

Figure 3.18. XRD results for $CaCO_3$ crystals precipitated in pure media and media supplemented with 50 and 100 ppm threonine. 60

Figure 3.19. FTIR results for $CaCO_3$ crystals precipitated in pure media and media supplemented with 50 and 100 ppm threonine 61

Figure 3.20. SEM images for $CaCO_3$ crystals acquired media supplemented with 50 ppm threonine at t = 30 min (a) and at t = 100 min (b).....63

Figure 3.21. SEM images for $CaCO_3$ crystals acquired media supplemented with 100 ppm threonine at t = 30 min (a) and at t = 100 min (b) 64

Figure 3.22. The change of zeta potential with time for threonine media. 65

LIST OF TABLES

Table 1.1. Amino acids. 12

Table 3.1. Filtration analysis results for tryptophan media 40

Table 3.2. Reaction mechanisms and symbols with their f(α) and g(α) 43

Table 3.3. Kinetic calculation results for thermal decomposition of $CaCO_3$ using the Coats–Redfern method.....45

Table 3.4. Experimental variables and their levels in central composite design matrix 46

Table 3.5. Central composite design matrix and results 46

Table 3.6. ANOVA results of the quadratic model for vaterite content 48

Table 3.7. Filtration analysis results for tryptophan media 58

Table 3.8. Filtration analysis results for threonine media.....66

1. INTRODUCTION

1.1. The Purpose of the Study

Calcium carbonate ($CaCO_3$) is one of the most abundant natural minerals, comprising approximately 5% of the Earth's crust. It has a wide range of potential applications in industry and biomineralization [1,2]. $CaCO_3$ takes various forms, including two hydrated crystal forms of ikaite ($CaCO_3 \cdot 6H_2O$) and monohydrate ($CaCO_3 \cdot H_2O$), an amorphous form, and three anhydrous crystalline polymorphs (calcite, aragonite, and vaterite) [3-5]. The most abundant form of calcite in nature is as a stable thermodynamic phase in rhombohedral crystalline shape [6]. Aragonite is metastable under ambient pressure and temperature and has a needle-like crystal shape with orthorhombic structure [7]. Vaterite is the thermodynamically least stable form of calcium carbonate and it has a hexagonal structure [8].

All three of these forms of $CaCO_3$ can be prepared by carbonation process under appropriate conditions and the order of abundance from high to low is calcite, aragonite, and vaterite in nature [9]. The vaterite polymorph is the least abundant in nature but it of particular interest for use in biomedical applications owing to its high specific surface area, good water solubility and dispersion, and lower density compared to the other two crystal polymorphs [10].

The properties of $CaCO_3$ are of particular importance in industrial applications, particularly the crystal structure, whiteness, chemical purity, specific surface area, particle size distribution, and morphology. Therefore, it is important to understand and have control of the different $CaCO_3$ polymorphs formed during crystallization, which has recently attracted growing research interest [11]. To the best of our knowledge, various physicochemical factors have been found to be responsible for the polymorphic phase transformation process of $CaCO_3$, such as temperature [12], solvent type [13], pH [14], and initial supersaturation [15]. In addition, different additives, such as barium, strontium, and magnesium ions [16,17], graphene oxide [18], biocompatible polymeric additives such as bovine serum albumin and polydopamine [19], selenic acid, arsenic acid, and silicic acid [20], and various types of amino acids [21], have been shown to greatly affect the morphology and polymorphic composition of $CaCO_3$ and the performance of the

resulting product. $CaCO_3$ polymorphism has been investigated previously but more work is needed to fully understand the factors that control the structure and morphology of $CaCO_3$ during its polymorphic transformation. Thus, in this study, we systematically investigated the effects tryptophan, glutamic acid, and threonine on the polymorphic phase transformation of $CaCO_3$. In order to better understand the polymorphic transformation process of $CaCO_3$, the structure, particle size, morphology, surface area and surface charge of the polymorphs were analyzed. Coats - Redfern method was employed to estimate the activation energy of $CaCO_3$ crystals and to ascertain the mechanism of thermal decomposition of $CaCO_3$. Moreover, experimental design was used to determine the effects of the process variables of temperature, stirring rate, and additive concentration on the transformation of $CaCO_3$ polymorphs. The novelty of this work lies in the use of a suitable experimental design to investigate the variables that affect the polymorphic transformation of $CaCO_3$ and any possible interactions between the variables to determine the optimum conditions for maximizing the vaterite content. This in-depth investigation of the effects of the interactions between the process variables on $CaCO_3$ crystallization will provide very useful information for industry and researchers.

1.2. Calcium Carbonate, Polymorphs and Properties

There is significant research interest in $CaCO_3$ because of its industrial importance, diversity as a biomineral, and crystalline complexity [22,23]. $CaCO_3$ is a mineral that is not found in pure form in nature and is not formed by organisms [24]. $CaCO_3$ dissolved in water is absorbed by some marine species and used in skeleton and shell structures. With the death of these creatures, the $CaCO_3$ in their structure's sediments in the seabed and the limestone formation process begins [25]. $CaCO_3$ is the main component of rocks in nature, in the form of stalactites and stalagmites, in the form of aqueous solution in the seas and oceans, in the skeletons and shells of animals and plants and constitutes more than 4% of the earth's crust [26,27].

$CaCO_3$ typically takes one of three crystal polymorph forms: calcite, aragonite, or vaterite [28]. Calcite is the most thermally stable polymorph in rhombohedral crystalline shape. Aragonite is metastable under ambient pressure and temperature and has a needle-like crystal shape with orthorhombic structure. Vaterite is the thermodynamically least stable

form of calcium carbonate and it has a hexagonal structure. The vaterite phase can be converted into the stable calcite phase under appropriate conditions [29,30]. Figures 1.1 and 1.2 illustrate the molecular structure and SEM images of the $CaCO_3$ polymorphs, respectively.

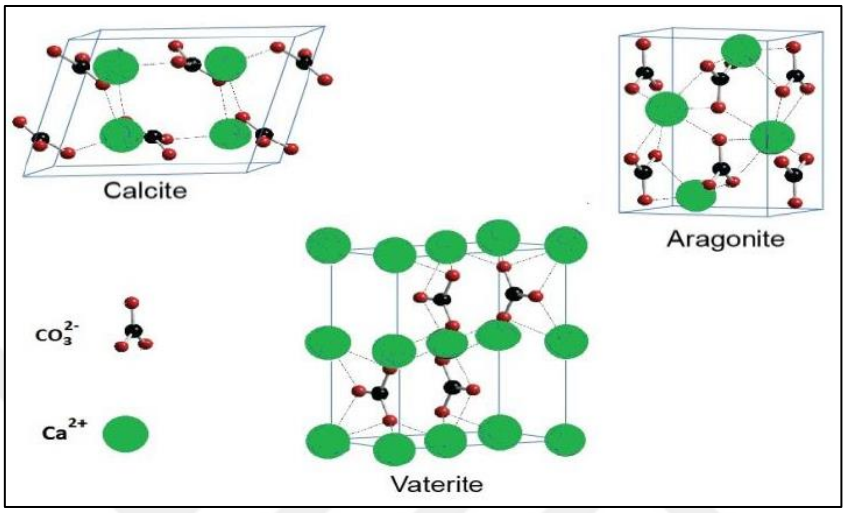

Figure 1.1. Polymorphs of calcium carbonate [31].

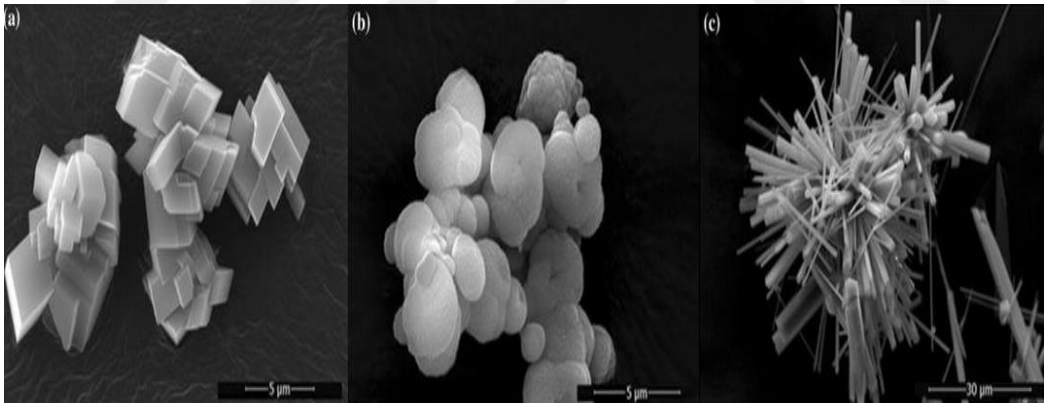

Figure 1.2. SEM images of the calcium carbonate polymorphs
a) calcite, b) vaterite and c) aragonite [32].

The properties of $CaCO_3$ crystals are determined by the crystal polymorph, size, and shape [9]. $CaCO_3$ is important in the oil/petrochemicals, water treatment, and energy production. Calcium carbonate is among the most common fillers applied in the pulp and paper industry because of its easy dispersibility and low propensity for agglomeration. Furthermore, $CaCO_3$ particles in the micrometer size range are used in the production of

plastics to reinforce polymers, improve their properties, and reduce production costs. In addition, fillers and pigments made using $CaCO_3$ crystals with small particle size have wide-ranging applications in the pharmaceutical and cosmetics industries, for example, as colorants, abrasives in toothpaste, and coatings for therapeutic delivery [33].

1.3. Polymorphism

Polymorphism is the ability of a material to exist in multiple crystal forms where the chemical structure remains the same but the molecular arrangement in the crystal lattice is different [34]. Although their chemical composition is the same, the two polymorphs are considered as two different compounds due to their different physical and chemical properties such as stability, particle size, crystal form, solubility, melting point, compressibility, and viscosity [35-36].

The term "pseudo-polymorphism" indicates substances involving a stoichiometric or non-stoichiometric amount of solvent in their crystal lattice. When water molecules are introduced into their crystal structures, they are referred to as solvates or hydrates. Similar to polymorphs, the various pseudo-polymorphs of a substance can have significantly different physical properties. However, pseudo-polymorphs become different chemical substances if solvents are added into their structures and thus, their physical and chemical properties may change [37]. A schematic representation of a polymorph and pseudo-pseudo-polymorph is presented in Figure 1.3 [38].

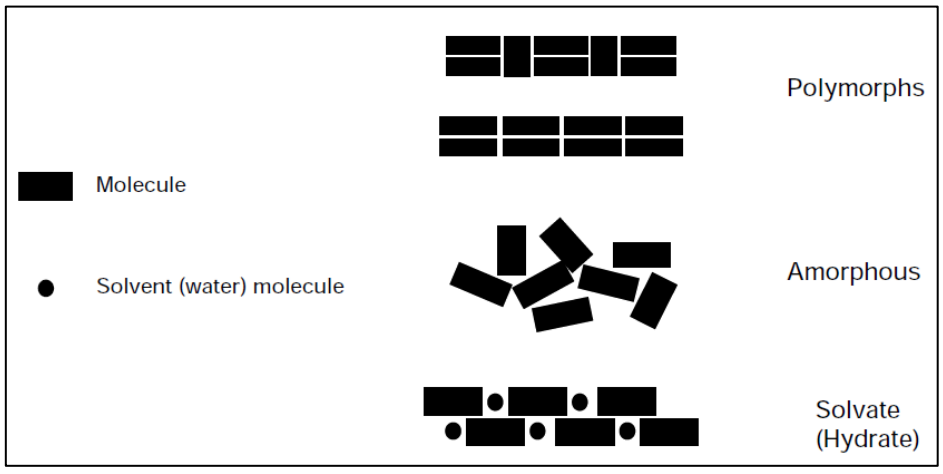

Figure 1.3. Schematic illustration of polymorphs and hydrate [38].

Polymorphs can be divided into two groups depending on their stability according to temperature and pressure range:

1. Enantiotropic polymorphs: One polymorph changes reversibly to another polymorph in temperature or pressure change.

2. Monotropic polymorphs: The exchange between two polymorphs is irreversible. As shown in Figure 1.4, the transformation of one polymorph to the other is reversible and occurs at the phase transition temperature T_τ.

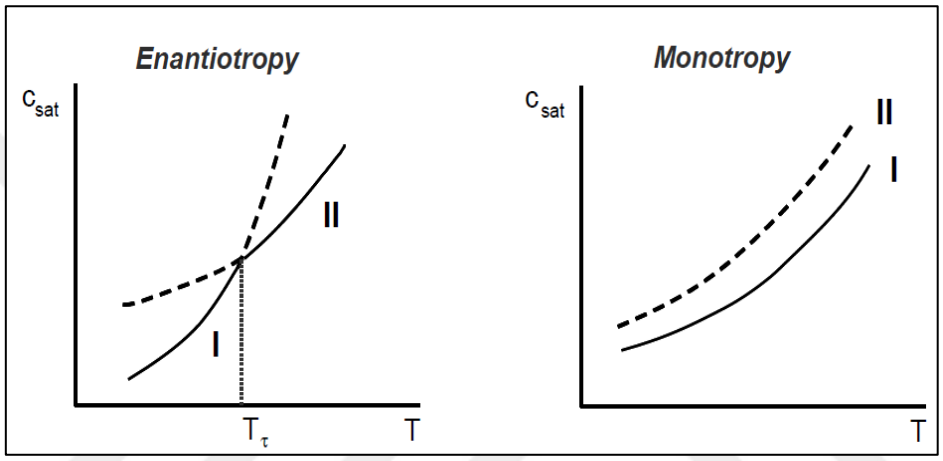

Figure 1.4. Solubility curves in case of polymorphy [38].

Enantiotropic phase transitions occur reversibly at the phase transition temperature. In the case of monotropy, one phase is all the time metastable in comparison with the other (form II with respect to form I). Consequently, non-intersecting resolution curves are formed [38].

If one of the polymorphs is stable at a definite temperature range and pressure and the other polymorph is stable at another temperature range and pressure, these two polymorphs are enantiotropic. In the case where only one polymorph is stable at all temperatures below the melting point, other polymorphs are unstable, the polymorphs are monotropic [39-40].

1.4. Crystallization

Crystallization is the process by which the crystal structure is formed. Crystallization can be defined as a phase change that is obtained as a product from solution and is used as a purification and separation technique in the production of many materials [41]. The

crystal obtained occurs in three dimensions depending on the structure of the substance and in space. The crystallization process takes place in three stages.

i) Supersaturation: Crystallization cannot occur before reaching supersaturation. Consist of supersaturation alone is not sufficient for crystallization.

ii) Nucleation: It is the event of formation of nuclei (solid surface) in the solution that has reached supersaturation and is a sufficient condition for crystallization.

iii) Crystal growth: It takes place in the growth of crystal particles formed in the supersaturated solution by the driving force of concentration. Mass transfer from the liquid stage to the solid stage enables this phenomenon to occur [42].

1.4.1. Supersaturation

The solution consists of a homogeneous mixture of two or more substances. There is a maximum amount that a certain amount of solvent can dissolve at a given temperature. The solution that reaches this amount is called saturated solution. The quantity needed to form a saturated solution under definite circumstances is called solubility [41]. A saturated solution is thermodynamically in equilibrium with the solid phase at a specified temperature. However, it is also possible to prepare solutions containing solids in excess of their saturation value. These solutions are called supersaturated solutions. These thermodynamically unstable solutions tend to return to an equilibrium state. This trend develops in proportion to the difference (ΔC) between the solution concentration and the saturation concentration. Briefly, ΔC constitutes the main effect both in the formation of nucleation and the growth of nuclei or crystals in the environment. Ostwald used the terms labile and metastable to classify supersaturated solutions with or without sudden nucleation [43]. Figure 1.5 shows the solubility supersaturation graph for a substance whose solubility increases with temperature. The solid line is the solubility curve. The curve given with the dashed line is the super-saturation curve, showing the temperatures and concentrations at which crystallization inevitably takes place. Although the location of the over-saturation curve cannot be determined precisely, there is a metastable region above the resolution curve so that the graph can be divided into three regions [42].

i) Stable zone: crystallization is impossible.

ii) Metastable zone: It is the part between the highest concentration values that a substance can reach at different temperatures under certain hydrodynamic conditions and

its solubility values. Here, without immediate nucleation, crystal growth can occur in the presence of a graft crystal in the medium. External factors affecting the metastable region include hydrodynamic conditions, mixing speed, physical purity of the solution, thermal history of the solution, cooling rate, ultrasonic noise, and the presence of additives.

iii) Labile zone: It is the instant crystallization zone [44].

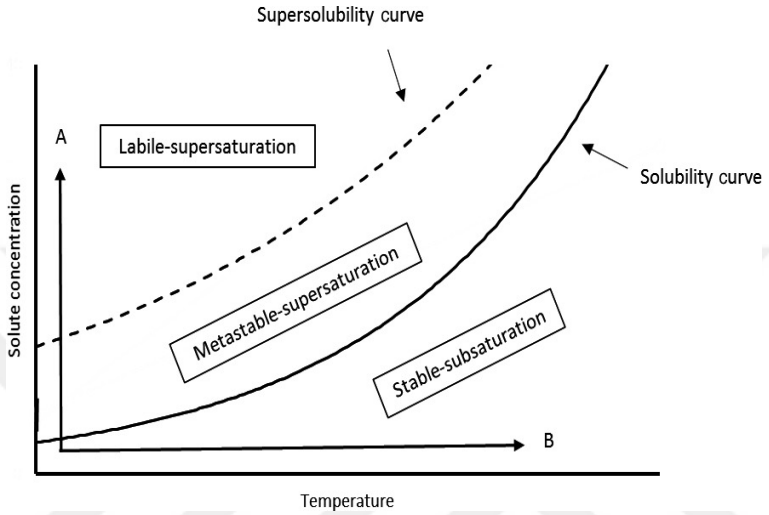

Figure 1.5. Solubility-supersaturation curve [42].

1.4.2. Nucleation

In order to form crystals, solid particles called nuclei or embryos are needed in solution to act as centers for crystallization. Nucleation can occur spontaneously or with an external effect. However, it is not always known whether nucleation occurs spontaneously or by an external effect. Nucleation is divided into two classes as primary and secondary nucleation [42,45,46]. Figure 1.6 shows the mechanisms of nucleation.

Primary nucleation involves systems not containing crystalline substances. Primary nucleation can be divided into two categories: homogeneous and heterogeneous nucleation [44]. Homogeneous nucleation is the form of nucleation formed by the formation of nuclei by itself, that is, by the assembly of molecules in supersaturated solutions. However, it is not known exactly how a stable crystal nucleus is formed in a supersaturated solution. Local concentration fluctuations cause nucleolus clusters. Most of these perish before they grow. If it reaches a certain size, it becomes stable. Homogeneous nucleation rate can be defined as the number of these crystallization centers formed per unit time and unit volume. Heterogeneous nucleation takes place in

the presence of foreign solid surface. Nucleation in such a system usually occurs at a lower oversaturation than in the homogeneous system. This is because a foreign substance in a supersaturated solution generally lowers the energy required for nucleation [42,45,46].

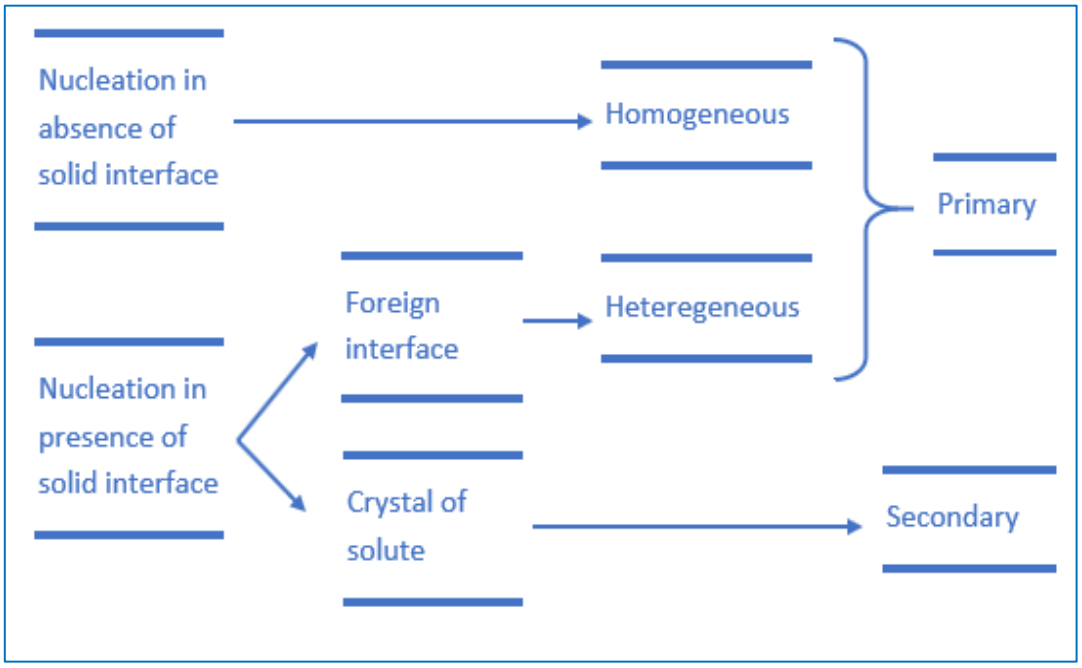

Figure 1.6. Nucleation mechanism [44].

Secondary nucleation occurs when crystals of solute material are found in a supersaturated solution. These crystals act as catalysts in the nucleation event, resulting in nucleation at a lower oversaturation than required for homogeneous nucleation. Despite many studies, very few of the kinetics and mechanism of secondary nucleation have been understood [44,46].

1.4.3. Crystal Growth

In a supersaturated system, stable nuclei begin to grow as soon as they form and become visible-size crystals. Crystal growth is a diffusion and coalescence process shaped by the surface of the crystal formed. Growth rate can be defined as the rate at which the crystal surface rises perpendicular to the surface. Crystal growth following nucleation controls the particle size distribution of the product obtained in the system. Growth rate and conditions are very effective in product purity and crystal habit [42].

1.5. Effects of Additives/Impurities on Polymorphism and Crystallization

Additives are substances that are added to the crystallization medium for a specific purpose (for example, to optimize the crystal structure or to reduce the crystallization rate). If a small amount of ingredients unintentionally affects the crystallization, it is called an impurity. However, there is no difference in their effects on the crystallization kinetics. Organic and inorganic additives and impurities play an important role in the crystallization process. All foreign molecules that show strong affinity at the crystal/ solution interface, even if present in very small amounts, significantly affect many properties of the crystallization process [47].

Among the many factors that affect the crystallization process (e.g., oversaturation, temperature, mixing), additives have the most influence. Even small amounts of additives can affect nucleation, crystal growth, crystalline shape, size, and other properties. An additive can be defined as a substance in the crystallization system that does not separate and precipitate as an additive under certain conditions. Additives are added to the solution to affect the product quality and parameters of the crystallization process and they are known to be effective in crystalline form and delaying crystal growth rates [48]. Most of the experimental studies are aimed to understand the additive effect, however, the properties in the structure and the form of crystal formation have also been studied [47].

Crystal growth occurs by binding appropriate molecular structures to active sites. Crystal growth continues with the binding of molecules in a stepwise way. Corners and steps are required for this growth. In the crystallization processes carried out in the presence of additives, these steps are held by the additive. In this case, the active adsorbent surface becomes deactivated. This is because the presence of foreign surfaces and particles requires a lower nucleation free energy. As a result, the crystal is prevented from growing and skipping steps [49].

Addition of additives to the crystallization process is also applied for the isolation of some phases of polymorphic substances. This method is used especially in the dye and pharmaceutical industry. Many products in these areas have more than one additive. By using additives, the transition of this polymorphic product from one crystal structure to another is prevented. An example is calcium oxalate. Calcium oxalate has more than one

crystal structure. Calcium oxalate trihydrate in aqueous solution does not have a stable structure, it turns into calcium oxalate monohydrate. In experimental studies, some additives such as organic phosphonic acids have been found to be effective in preventing this transformation [50].

1.6. Amino Acids

Amino acid is a compound that contains both an amine group ($-NH_2$) and a carboxyl group ($-COOH$) in the same molecule. Amino acid is the building blocks of proteins. It consists of nitrogen, carbon, hydrogen and oxygen, and it is also organic compound that contains a variable side chain group in its structure [51]. The R group in the structure of amino acids; the straight chain or branched aliphatic group can be an aromatic or heterocyclic ring or hydrogen [52]. Basic structure of an amino acid is shown in the Figure 1.7.

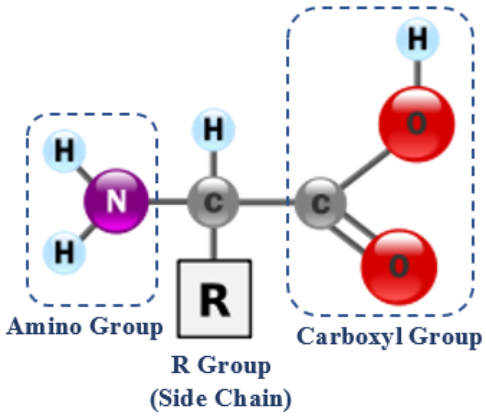

Figure 1.7. The structure of amino acid.

Four different groups are attached to the four valences of a carbon atom in the structure of amino acids. Three of these groups (-COOH, $-NH_2$ and -H) are unchanged. The R group attached to the fourth valence of the carbon atom changes, allowing the derivation of various amino acids. The R group is called the side chain of the amino acid. There are different types of amino acids in nature. 20 of these are called standard amino acids [52].

The first amino acid discovered was the asparagine amino acid, which was isolated from the plant called asparagus in 1806. Studies on the investigation of the properties of amino

acids started after the synthesis of the first amino acid. The first amino acid synthesized was glycine, and it was isolated by Braconnot in 1820 from hydrolysis of a protein. Since amino acids other than glycine have asymmetric carbon atoms in their structures, they are optically active compounds that can turn polarized light to the right or left. Amino acids are in D- or L-form, and they found in living organisms have the L configuration.

Amino acids are found in neutral solutions in the form of dipolar ion (inner salt) formed by the shift of the proton (H +) in the carboxyl group to the nitrogen atom. When acid is added to these solutions, the proton will be attached to the carbonyl anion, thus forming a cation. If base is added, the anion is formed when the ammonium cation gives proton to the hydroxyl ion. The buffering effect of proteins in the blood is due to these amphoteric properties of amino acids. Due to the amphoteric properties of amino acids, they form compounds in salt structure as a result of their reactions with acidic and basic solutions [53,54].

Table 1.1. Amino acids.

Name	Molecular Formula	Structural Formula	Abbrevations
Alanine	$C_3H_7NO_2$	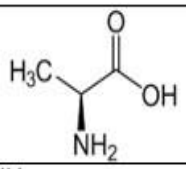	Ala, A
Arginine	$C_6H_{14}N_4O_2$	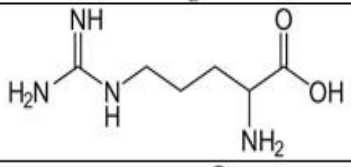	Arg, R
Asparagine	$C_4H_8N_2O_3$	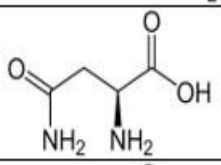	Asn, N
Aspartic acid	$C_4H_7NO_4$	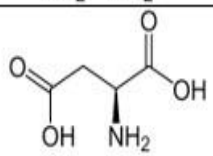	Asp, D
Cysteine	$C_3H_7NO_2S$	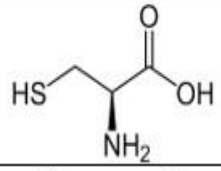	Cys, C
Glutamic acid	$C_5H_9NO_4$	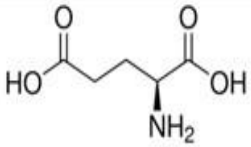	Glu, E
Glutamine	$C_5H_{10}N_2O_3$	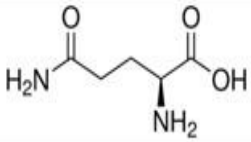	Gln, Q
Glycine	$C_2H_5NO_2$	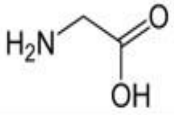	Gly, G
Histidine	$C_6H_9N_3O_2$	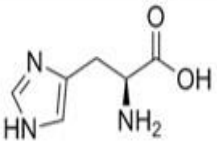	His, H
Isoleucine	$C_6H_{13}NO_2$	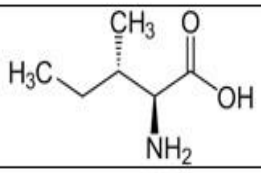	Ile, I

Table 1.1. Continued.

Leucine	$C_6H_{13}NO_2$	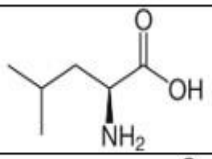	Leu, L
Lysine	$C_6H_{14}N_2O_2$	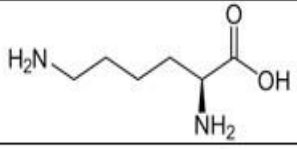	Lys, K
Methionine	$C_5H_{11}NO_2S$	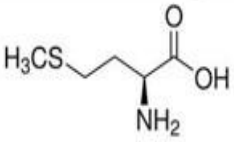	Met, M
Phenylalanine	$C_9H_{11}NO_2$	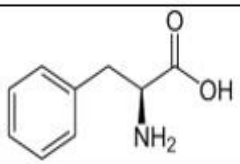	Phe, F
Proline	$C_5H_9NO_2$	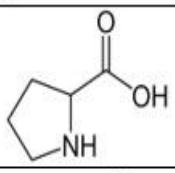	Pro, P
Serine	$C_3H_7NO_3$	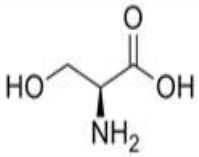	Ser, S
Threonine	$C_4H_9NO_3$	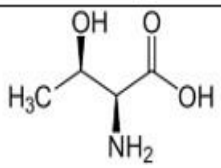	Thr, T
Tryptophan	$C_{11}H_{12}N_2O_2$	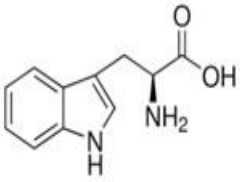	Trp, W
Tyrosine	$C_9H_{11}NO_3$	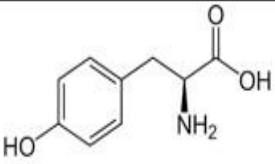	Tyr, Y
Valine	$C_5H_{11}NO_2$	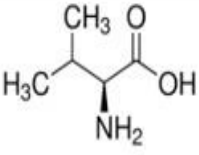	Val, V

1.6.1. Tryptophan

Tryptophan is an essential type of amino acid required to produce niacin (vitamin B3). It is needed by all life forms for protein synthesis and different important metabolic functions [55]. Figure 1.8 shows the molecular structure of the tryptophan.

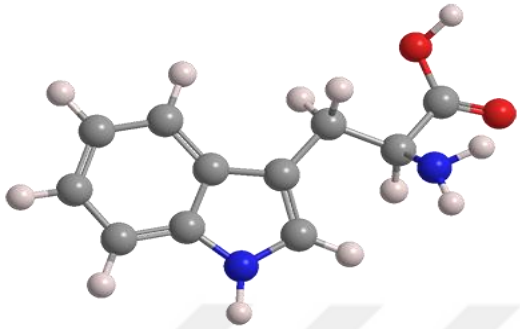

Figure 1.8. Molecular structure of tryptophan.

1.6.2. Glutamic Acid

Glutamic acid is an α-amino acid that is used by almost all living beings to form proteins. Figure 1.9 shows the molecular structure of the glutamic acid.

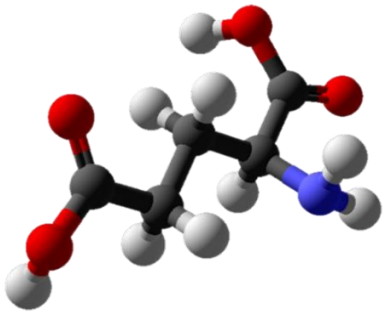

Figure 1.9. Molecular structure of glutamic acid.

Glutamic acid is used in various fields. This amino acid group is used especially in the food industry, cosmetics industry, medical field, water treatment processes and fertilizers which are agricultural products. There are many different uses of glutamic acid in the food industry. It is used as a thickener in liquid foods. It is used as an additive in bakery products. Glutamic acid is applied in various procedures and studies in the medical and

health field. It can be used in medical applications due to its properties such as helping the patient in osteoporosis conditions, increasing calcium absorption, and being a biocompatible carrier in the treatment of cancer drugs [56].

1.6.3. Threonine

Threonine is an essential amino acid that is chemically α-amino β-hydroxybutyric acid. It is found in many proteins in the form of O-phosphotreonine [57]. Figure 1.10 illustrates the molecular structure of the threonine.

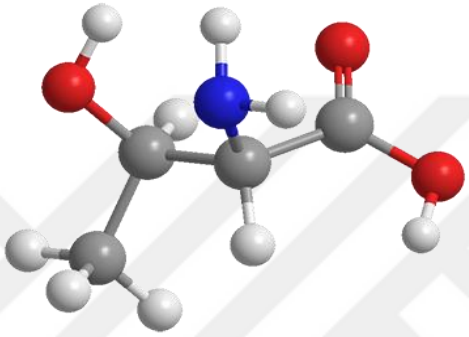

Figure 1.10. Molecular structure of threonine.

1.7. Studies About Calcium Carbonate Polymorphism

According to the literature research, there are lots of studies about $CaCO_3$ crystallization and polymorphic phase transformation. In the below, relatively recent studies about $CaCO_3$ polymorphism were explained.

Lin et al. [58] investigated the effects of the microbial metabolism on the $CaCO_3$ crystallization and polymorph selection. The influences of microbial sulfate reduction on $CaCO_3$ polymorphism were studied by utilizing pure culture of sulfate reducing bacteria called *D.bizertensis*. Transformation of $CaCO_3$ polymorphs was also investigated under these conditions. Different Mg/Ca ratios (0:1, 1:1, 2:1, 3:1, 4:1, 5.2:1, 9:1) were used for incubation of *D.bizertensis* with different seeding materials. The experiments for transformation of monohydrocalcite (MHC) were carried out at 100°C. Experimental results showed that MHC (monohydrocalcite) and calcite were observed as a precipitated polymorph from all experiments. MHC crystals were dominant in all solutions with

Mg/Ca ratio of greater than 3 while calcite formed in the media with an initial Mg/Ca ratio of 1 or less. According to the transformation experiments, it was also stated that MHC transformed into calcite and aragonite in pure sea water while it transformed into only calcite when incubated with pure MQ-water. On the other hand, there was no transformation into a more stable calcium carbonate polymorph observed within media containing sea water with yeast extract or inorganic phosphate.

Hu et al. [14] studied the impact of pH and phosphate on the $CaCO_3$ polymorphism were investigated. pH effect was investigated for two different pH values which were 9 and 13.4, respectively. The effect of PO_4 whose concentration varied from 0 to 10 μmol/L was also tested for each experimental condition including different Ca/CO_3 ratios of 1:1 and 10:1 at different pumping rates (from 3.6 to 100 μL/min). Experiments were performed at near-freezing temperature (0-0.5 °C) by utilizing double walled water jacket connected to water-bath. pH adjustment was controlled by using NaOH solution during the experiments. The optical images and Raman spectroscopy were used for phase identification of $CaCO_3$ crystals. Experimental results indicated that two forms of $CaCO_3$ were observed in this study which were ikaite and vaterite. Also, it was clearly stated that pH and phosphate had a significant impact on transformation between ikaite and vaterite. Vaterite was the predominantly precipitated polymorph of $CaCO_3$ in absence of phosphate in this study. However, ikaite formation was favored over vaterite at moderate alkaline condition in presence of phosphate while ikaite formation was triggered without phosphate requirement at high alkaline solution. Thus, according to the these results it was indicated that phosphate could contribute to transformation of vaterite to ikaite at low temperature and moderate pH 9.0. On the other hand, phosphate did not have impact on transformation behavior of polymorphs at high alkaline condition (pH 13.4) due to the enough driving force of high alkalinity to trigger the ikaite formation.

Stajner et al. [21] researched the impact of various amino acids such as Asp, Lys, Asn, Tyr, Phe, Ser, Ala on spontaneous precipitation of $CaCO_3$ polymorphs were investigated. The experiments were carried out at 25 ° C in a double walled thermostatic glass vessel by mixing equal volume of $CaCl_2$ and Na_2CO_3. After precipitation experiments, obtained crystals were analyzed by different characterization techniques. On the other hand, selected amino acids influenced $CaCO_3$ precipitation in different way. Phe and Ala having non-polar side group had no significant effects on the precipitated solid phases. Asp had

the strongest impact on the calcite morphology for its all concentrations. But only calcite crystals were observed for high concentrations of Asp whereas its lower concentrations promoted the vaterite formation.

Siva et al. [59] investigated the influence of polyethylene glycol (PEG) on the formation of $CaCO_3$ particles. The experiment with PEG was performed by mixing $CaCl_2$ and PEG at 60 °C and then continued with adding of Na_2CO_3 and cooling down of the mixture to room temperature for precipitation. Also, $CaCO_3$ precipitation without PEG additive was performed for controlling. The obtained crystals were analyzed using FTIR, XRD, SEM and particle size distribution analysis. According to the experimental result, it was clearly observed that PEG had a significant effect on the $CaCO_3$ crystallization. Therefore, PEG molecules got adsorbed over $CaCO_3$ crystals and as a result crystal growth rate and crystal activities. Hence, it was clearly stated that addition of PEG led to aragonite and vaterite formation while calcite crystals was observed without PEG. Also, length of PEG molecular chained had effect on the crystal formation. The increment of the molecular weight of PEG (PEG3200, PEG8000) could lead to increment of solution viscosity, adsorption layer thickness and electrostatic interaction between PEG and $CaCO_3$ crystals. Thus, this led to aragonite and vaterite formation rather than the calcite formation due to its inhibition effect on it.

Sarkar and Mahapatra [60] investigated the $CaCO_3$ polymorphism without the additives and presented a new procedure to synthesize all three $CaCO_3$ polymorphs at ambient temperature conditions. They found that the vaterite gradually transformed into aragonite. They reported that this conversion occurs faster if the vaterite specimen is refluxed in distilled water. In both cases, they observed that the aragonite formed was stable and there was no conversion to calcite even when it was poured into the main filtrate.

Aquilano et al. [61] studied the effects of impurity on $CaCO_3$ polymorphism and crystal growth. The specific effect of serial epi-adsorption of appropriate foreign species on the change of the balance and growth patterns of the crystals was investigated by providing impurities with the addition of Li^+ as lithium chloride to the calcium carbonate solution. As a result of the experiments, it was observed that an interaction occurred between the polymorphs and lithium.

Juhasz-Bortuzzo et al. [62] studied the effect of ultrasound on controlled particle size vaterite formation for using in medical applications. The research was performed in an alkaline medium and the temperature was kept below 30 °C using traditional mixing method and applying different ultrasound amplitudes and durations. The properties of the particles were determined by XRD, FTIR, SEM and TEM analyzes. It was observed that the ultrasound synthesis process caused the formation of vaterite with a smaller size compared to the traditional mixing method, as well as shortening the crystallization time by increasing the crystallization rate. With increasing ultrasound power and time, the particle size of the particles was diminished and the synthesis of nano powder $CaCO_3$ with a stable structure was achieved. It was found that decreasing temperature, high ultrasound intensity and short ultrasound duration were effective in the reduction of the vaterite size.

Yao et al. [63] investigated the effects of amino acids on $CaCO_3$ crystallization process. Aspartic acid and arginine, types of polar amino acids, were used as organic templates to induce $CaCO_3$ growth. The relationship about the growth of carbonate crystals in the agarose gel and amino acid system at different concentrations was investigated. XRD and SEM analyzes were carried out to determine the precipitation phase of the formed crystals and to determine morphological properties of the crystals. As a result, it was reported that amino acids played an important role in the biomineralization process of $CaCO_3$, the presence of Arginine supported the formation and growth of calcite crystals, and the presence of Aspartic acid helped the formation and growth of vaterite crystals.

Korchef [64] studied the effects of iron ions on the $CaCO_3$ crystals in a CO_2 system. The condition was set at 28 °C and pH 6. Experimental results showed that iron ions had a significant effect on calcium carbonate in terms of supersaturation. The addition of iron ions at low supersaturation delayed $CaCO_3$ nucleation and increased the crystal growth rate after the initiation of nucleation. On the other hand, iron ions did not have a critical effect on $CaCO_3$ in high solution supersaturation. Increasing the initial concentration of iron ion had a supportive effect on vaterite formation.

1.8. Characterization Techniques

1.8.1. X-ray Diffraction Analysis (XRD)

X-rays were found and named in 1895 by the German physics professor Wilhelm Konrad Roentgen. X-rays are short wavelength and high energy rays that form a part in the electromagnetic spectrum between Gamma rays and ultraviolet rays. It was discovered that X-rays are diffracted by crystal planes by Laue in 1912. Later, W. H. Bragg laid the foundations of crystallography with the equation. This equation, known as the Bragg equation of X-Rays, is formed with the logic that the angle and length of the incident X-rays change depending on the distance between the atomic layers making up the crystal structure. By recording these refracted rays in the detector, the number and order of layers of the target crystal can be understood.

$$2d \sin\theta = n\lambda \qquad (1.1)$$

The theory developed by W. L. Bragg is the most widely used theory of X-ray diffraction. X-rays with 'λ' wavelengths scattered from crystal planes with a distance of 'd' between them form the angle. The experimental parameter, 2θ, is the angle between the scattered and continuing X-ray's beam. The distance between all crystal planes parallel to each other is 'd'.

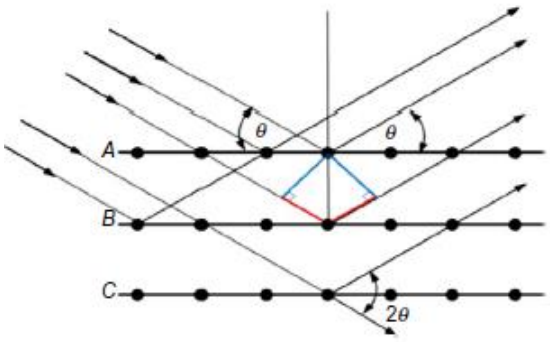

Figure 1.11. Schematic representation of reflections from adjacent planes within the crystal [65].

When a dense beam of X-rays strikes a crystalline structure consisting of regular atom groups, a general scattering occurs, and these scattering beam waves affect each other and annihilate each other by interfering. However, at certain angles, these waves increase the wave intensity by combining with one another in a phase. This formation is known as diffraction of X-rays. These directions in which diffraction occurs vary depending on the size and shape of the crystalline unit cell. The intensity of diffraction is determined by some structural properties of the crystal. Figure 1.12 shows a simple X-ray diffraction experiment diagram.

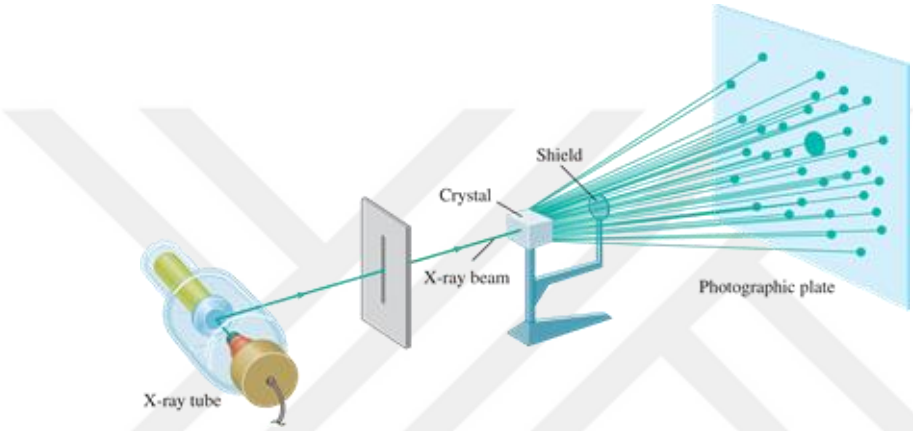

Figure 1.12. Diagram of a simple X-ray diffraction experiment.

X-rays are generally caused by the impact of an electron beam on matter. In order to emit X-rays, electrons must have a certain energy. This electron beam is created by heating a filament in a vacuum, and a voltage applied between the cathode and the anode [65-68].

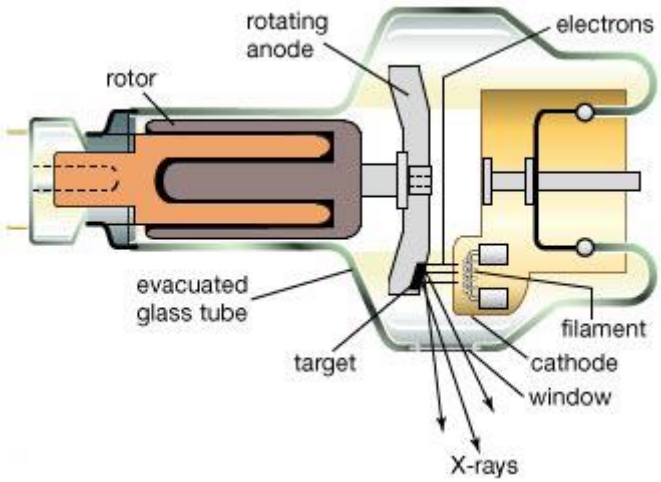

Figure 1.13. X-Ray tube.

1.8.2. Fourier Transform Infrared Spectrophotometer (FTIR)

The Fourier Transform Infrared Spectroscopy is an analytical equipment that used to collect high spectral resolution data over a wide range by measuring the number of waves against the infrared intensity of light with mathematical Fourier transform [69-71]. Infrared (IR) spectroscopy is a tool used to characterize organic or inorganic compounds. FTIR Spectroscopy is based on the principle of measuring the absorption of infrared (IR) radiation and the vibration of chemical bonds. Each functional group has its own vibration frequency, and each infrared spectrum is specific [72,73].

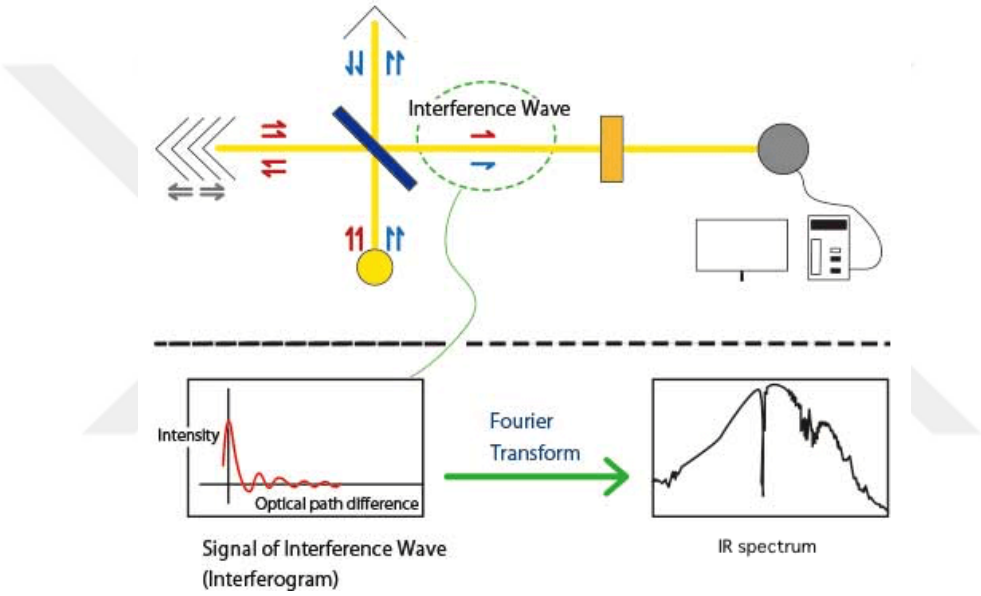

Figure 1.14. Schematic representation of Fourier transform infrared spectroscopy.

1.8.3. Scanning Electron Microscopy (SEM)

In the scanning electron microscope, surface is scanned with a focused beam of electrons and an image is obtained. The signals, resulting from the interaction of electrons with atoms on the sample surface, contain information about the surface topography and composition of the sample. These signals are collected by the relevant detectors and transferred to the computer screen and the image is obtained. Figure 1.15 shows the schematic representation of SEM.

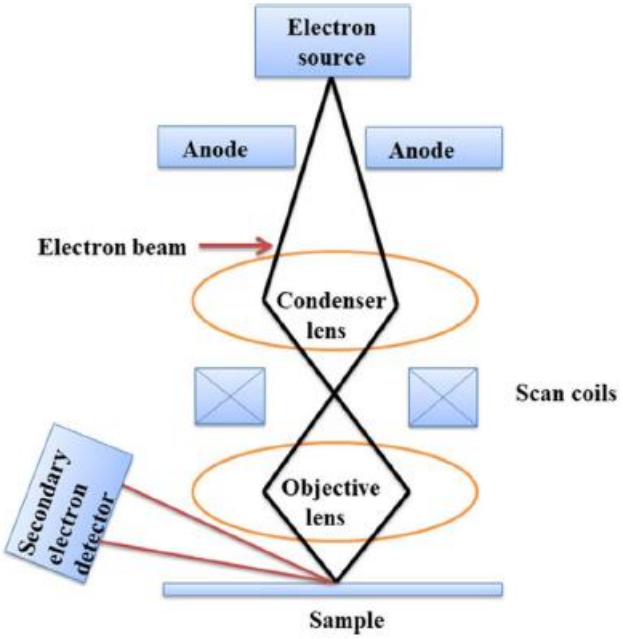

Figure 1.15. The representation of SEM [74].

In the optical column of the SEM; there are the electron gun, which is the source of the electron beam, the anode plate where high voltage is applied to speed up the electrons towards the specimen, condenser and objective lenses used to collect and direct the beam, apertures used to limit the beam diameter, scanning coils that deflect the beam properly to scan the sample surface. The optical column opens from the bottom to the sample chamber. Here, there are sample cradle that can move in three dimensions, sensors sensitive to different signals resulting from beam-sample interaction. The electronic equipment of the microscope creates images that reflect the different properties of the sample by processing the signals from the sensors, while keeping the filament current, lens current and excitation voltage stable [74-77].

1.8.4. Atomic Force Microscopy (AFM)

Atomic force microscope (AFM) obtains three-dimensional topographic images of the material surfaces by scanning the surface with a fine tip. It is used to obtain various surface properties and physicochemical surface properties of low-size nanostructures and nanomaterials for all kinds of solid materials. Scanning is done by the voltage supplied to the piezoelectric material. Due to the interaction force between the sample and the

scanning tip, deviations occur in the tip-spring system. These deviations are determined by optical or electrical methods and then sent to the feedback mechanism and used as a reference while obtaining the image. Figure 1.16 shows the schematic representation of AFM.

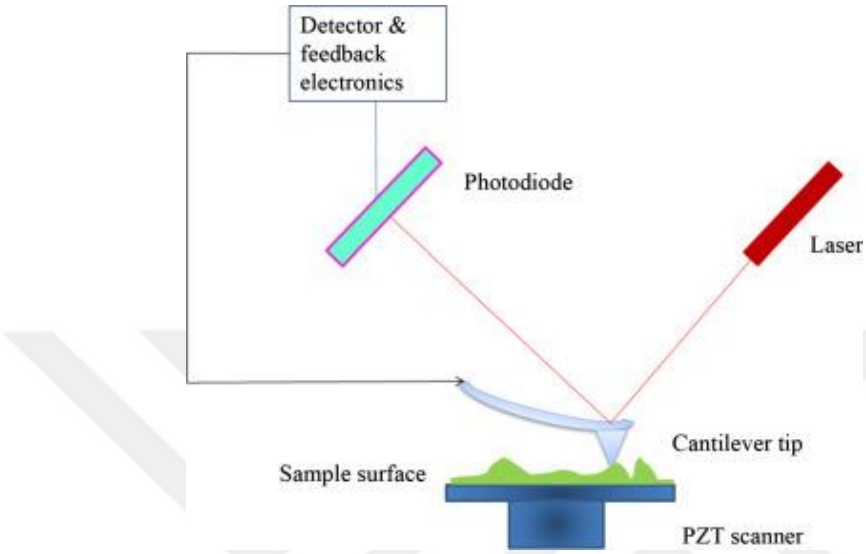

Figure 1.16. Schematic representation of atomic force microscope [74].

When the tip used to scan the specimen surface in AFM gets close sufficiently to the surface, the forces of attraction between the surface and the tip cause the rod to deviate towards the surface. As the tip comes closer to the surface, as it touches the surface, the thrust enhances, and the rod diverges from the surface. Rod deflections towards or away from the surface are catched with the help of a laser beam. The laser beam reflects off the rod-like equipment. If the rod moves, alterations will also occur in the angle of the reflected beam. Position sensitive photo diode (PSPD) is used to catch these alterations. With these deviations in the laser beam, the investigated nanoscale surface indentations and projections are recorded. AFM is used in a multifarious of natural science fields such as molecular engineering, solid-state physics, surface chemistry, semiconductor technology, cell biology, and medicine etc. [78-80]. Figure 1.17 shows some images obtained from AFM analysis.

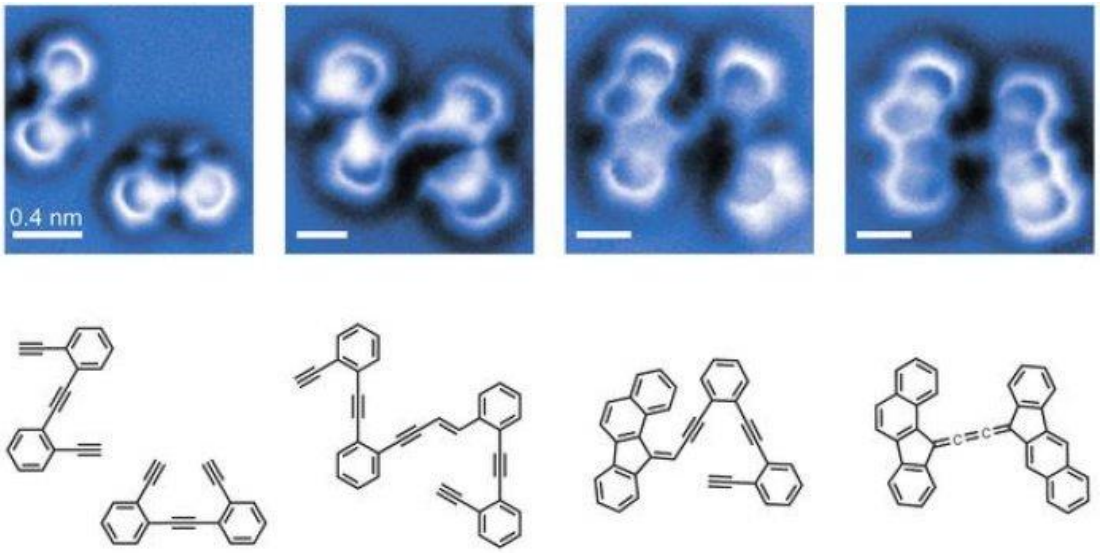

Figure 1.17. Images obtained by AFM.

1.8.5. Zeta Potential

Zeta potential refers to the surface charge of solid particles on the shear plane within the electrical double layer and is certainly less than the surface charge of the particle itself. For this reason, zeta potential can also be expressed as "measurable surface load of the particle". The main reasons why solid particles gain surface load in water or liquid are as follows:

- Ionization (dissociation) of functional groups such as carboxyl (-COOH), hydroxyl (-OH) amine ($-NH_2$) on the particle surfaces.
- From the preferential dissolution of the lattice ions forming the crystal structure.
- By the replacement of high valence cations by low valence cations during the formation of the crystal structure.
- Bond breaks and crystal structure defects that occur during size reduction processes.
- From preferential adsorption of some ions in suspension.
- From accumulation of electrons at the solid surface or at the solid-liquid interface or from the deposition of molecules with a dipole structure.

The most important cause for detection the zeta potential value is to determine the size of the diffuse double layer surrounding the particle. The zeta potential enables many important properties of colloidal systems to be understood and controlled, and to determine the electrical charge or potential on the particles. Measurement of zeta potential is also crucial to understanding dispersion and aggregate processes [81-86]. Figure 1.18 shows the visualization for electrical double layer of a particle suspended in a liquid.

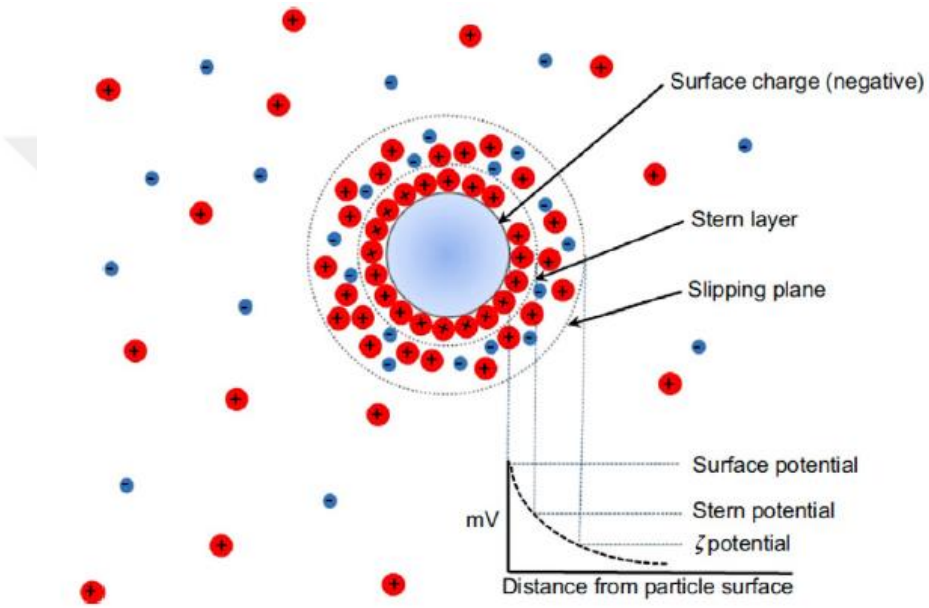

Figure 1.18. Visualization for electrical double layer of a particle suspended in a liquid [81].

1.8.6. Thermogravimetric Analysis (TGA)

In thermogravimetric analysis, the mass of the heated sample is measured as a function of time or temperature. In this analysis, a graph is drawn between the measured mass change and temperature. The graph obtained is expressed as mass loss curve/thermal degradation curve/thermogram. Such graph includes mass in the ordinate and time or temperature in the abscissa. Thermograms can be recorded at a single heating rate or multiple heating rates. The effect of thermal energy on the sample mass can be determined with the graphics obtained. In addition, the composition and stability of the intermediate

product and residue, if any, can be determined. Thanks to these thermograms, information about the chemical reaction mechanism and thermodynamics of the sample can be obtained.

In order to examine the material by thermogravimetric method, a change occurs in the material mass with the effect of temperature. In some cases, transformations that produce energy changes may not produce mass changes. In these cases, no results can be obtained in thermogravimetric analysis. The resulting mass change occurs when the physical or chemical bonds of the material are broken, or bonds are formed at high temperatures. The removal of volatile components from the sample or separation from the substance causes the mass to change. It is not possible to examine the phase changes in which the mass does not change by thermogravimetric analysis.

Thermogravimetric analysis can be used to elucidate stoichiometric deterioration related to decomposition reactions, drying process, pyrolysis in inert atmospheres or oxidative energy loss in oxygen/air. More precise results can be reached with the curves obtained by taking derivatives of thermograms.

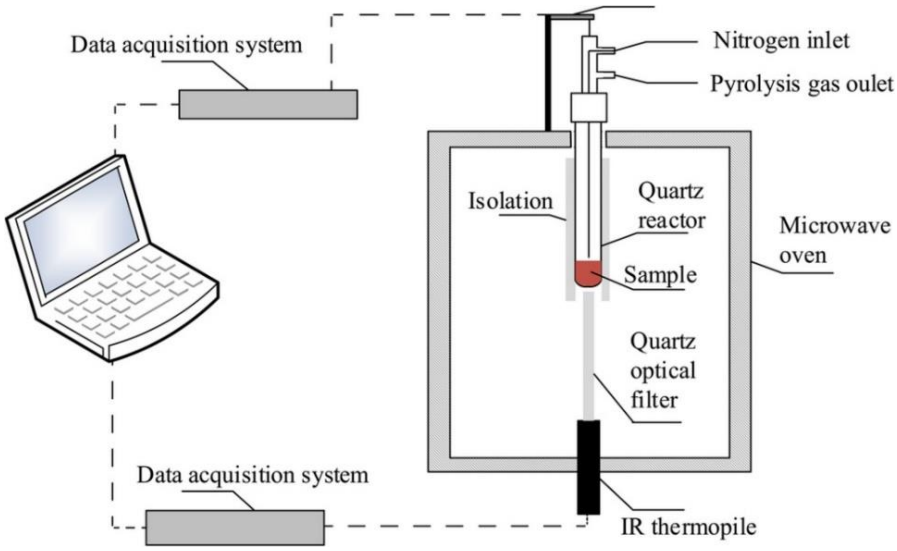

Figure 1.19. Schematic representation of thermogravimetric analysis [87].

In thermogravimetric analysis, the material is heated in the furnace in the crucible according to a certain temperature program and the mass change is recorded continuously.

The beam from a single source passes through a thin hole and falls on a pair of photocells. The beam intensity falling on the photocells is equal to each other when the balance is in stable. Thus, the beam intensity falling on the photocells is changed. The change signal oxidized by the electronic circuit is sent to the recorder. The obtained signal is a measure of the loss of mass in the sample. In addition, by sending the difference signal to the moving winding in the balance arm, the balance is brought into balance again [87-89].

2. MATERIALS AND METHOD

2.1. Materials

Analytical-grade calcium chloride dihydrate ($CaCl_2 \cdot 2H_2O$), sodium carbonate (Na_2CO_3), tryptophan ($C_{11}H_{12}N_2O_2$), glutamic acid ($C_5H_9NO_4$), and threonine ($C_4H_9NO_3$) were purchased from Merck. All solutions were prepared using distilled water.

2.2. Experimental Method

The polymorphic phase change of $CaCO_3$ was performed using the setup shown in Figure 2.1. $CaCO_3$ was prepared by the reaction between $CaCl_2 \cdot 2H_2O$ and Na_2CO_3 in a glass crystallizer with an active volume of 1.0 L.

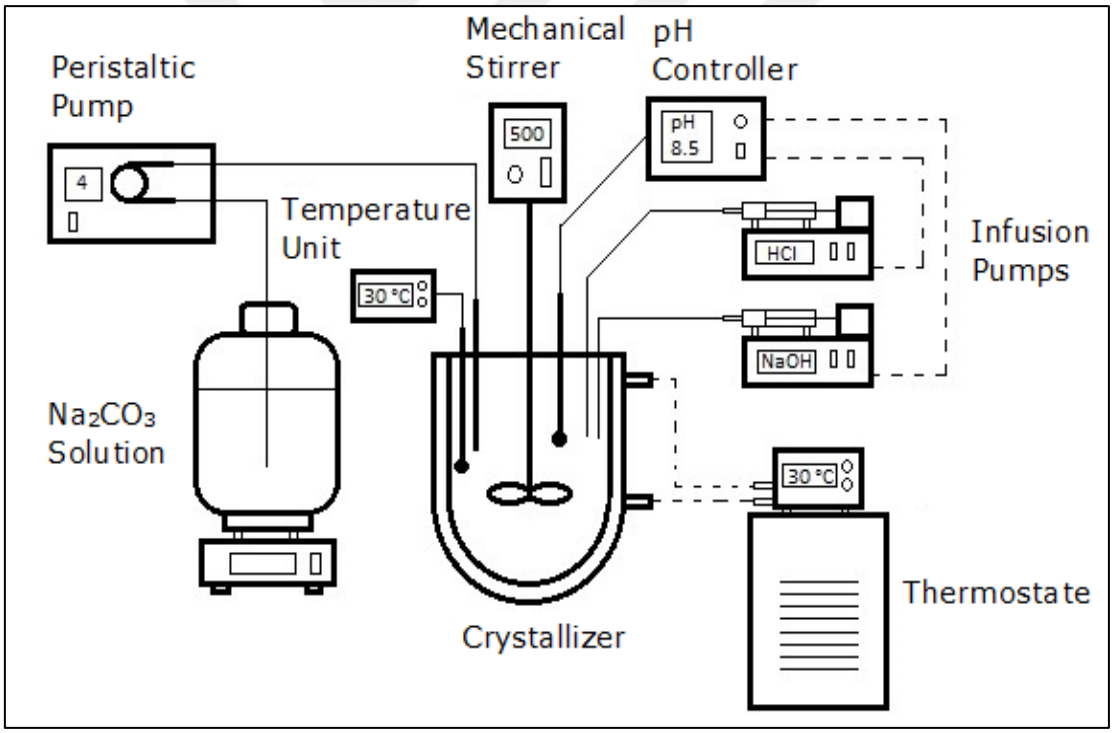

Figure 2.1. The experimental setup.

The synthesis process is as follows. At the beginning of the experiment, 0.2 M calcium chloride solution (0.4 L) was placed into the crystallizer. After thermal equilibrium was reached, a 0.2 M sodium carbonate solution (0.4 L) was fed into the crystallizer at a rate of 4 mL/min using a peristaltic pump. The suspension in the crystallizer was stirred at a

rate of 500 rpm. During the polymorphic transformation process, the pH of the solution was continuously monitored via a pH probe inserted into the crystallizer and maintained at pH 8.5 by the addition of 0.1 N HCl (aq) and 0.1 N NaOH (aq) by an automatic pH control system. The suspension temperature was maintained at a 30 ± 0.1 °C. At 30 and 100 mins, 20-mL aliquots of the suspension were removed and used for crystal structure and morphology analysis.

The effect of tryptophan, glutamic acid, threonine and their concentrations on the polymorphic transformation of $CaCO_3$ was investigated in this study. The specific amount of the tryptophan, glutamic acid, and threonine (corresponding to 50 ppm and 100 ppm) was added into the crystallizer at the beginning of the experiment. The product obtained was collected, filtered by using 0.45 μm membrane filters, washed with distilled water, and finally dried at room temperature. The prepared samples were treated prior to further analysis.

2.3. Analysis

The precipitated $CaCO_3$ were analyzed for structure, functional group, crystal size, morphology, surface charge and thermal characteristics. Firstly, X-ray diffraction (XRD, Bruker D2 Phaser Table-top Diffractometer) was used to determine the phase structures of the $CaCO_3$ polymorphs and scanned in the range of 10 to 70° with a scan rate of 3°/min. The calcite and vaterite polymorphs in the $CaCO_3$ were quantitatively determined using the Rietveld refinement method. Meanwhile, the polymorphic transformation was monitored by Fourier transform infrared spectroscopy (FTIR; Shimadzu IR Affinity-1). The spectra were recorded with scanning range from 600 to 2000 cm^{-1} at room temperature. The crystal morphologies of the $CaCO_3$ were investigated by scanning electron microscopy (SEM/EDX; Zeiss EVO LS 10) and the particle size distributions were measured with a Malvern Mastersizer 2000 instrument. Zeta potential measurements were conducted using a Malvern Zeta Sizer Nano Series Nano-ZS. The thermal behavior of the $CaCO_3$ precipitated in pure and additive media was determined using a Setaram LABSYS Evo thermogravimetric analyzer in a nitrogen atmosphere between 50 °C and 950 °C with a heating rate of 10 °C/min. Using the obtained data, the thermal decomposition kinetics for the $CaCO_3$ crystals precipitated in pure media were investigated and the kinetic parameters were calculated.

3. RESULTS AND DISCUSSION

3.1. The Results of Effects of Tryptophan on the Polymorphic Transformation of Calcium Carbonate•

3.1.1. XRD Analysis

The XRD patterns of the samples at 30 and 100 min during the polymorphic transformation process from calcite to vaterite in the presence of 50 ppm and 100 ppm tryptophan are shown in Figure 3.1. The XRD results indicate that the $CaCO_3$ crystals precipitated in pure media were only in calcite form (JCPDS: 05-0586) and no intermediate phase was produced in pure media. The main peaks observed at 2θ of 23.1°, 29.4°, 35.9°, and 39.3° are diffraction peaks corresponding to the calcite crystals lattice planes of (012), (104), (110), and (113), respectively. When 50 ppm tryptophan was added to media, the resulting crystals included both calcite and vaterite forms together. The solid sample taken at 30 min showed the appearance of new peaks at 2θ = 21.0°, 24.9°, 27.1°, 32.7°, and 50.1°, which were assigned to the (002), (110), (112), (114), and (118) lattice faces of vaterite, respectively (JCPDS: 33-0268). Rietveld refinement quantitative analysis determined the calcite and vaterite contents to be 74.84% and 25.16%, respectively, for the 30-min sample obtained from media supplemented with 50 ppm tryptophan. As the transformation process progressed further, more of the vaterite form (41.20%) was found in the crystal sample. The intensity of the characteristic diffraction peaks of vaterite was obviously increased and more of the vaterite polymorph was obtained with time.

When the tryptophan concentration was 100 ppm, both calcite and vaterite diffraction peaks were observed in the solid sample obtained at 30 min during the polymorphic transformation process and the mass fractions of calcite and vaterite were calculated to be 61.26% and 38.74%, respectively. The results of Rietveld refinement quantitative analysis showed that the vaterite content increased with the increasing tryptophan concentration. In the sample obtained at 100 min, the characteristic diffraction peaks of calcite had completely disappeared, showing that all the calcite crystals were completely

• Polat, S., Ozalp-Sendur, T.N., Sayan P. (2021) Effects of Tryptophan on the Polymorphic Transformation of Calcium Carbonate: Central Composite Design, Characterization, Kinetics, and Thermodynamics, Acta Chimica Slovenica, Accepted-In press.

transformed into the vaterite form. The XRD results indicated that tryptophan influenced the crystal structure of calcium carbonate.

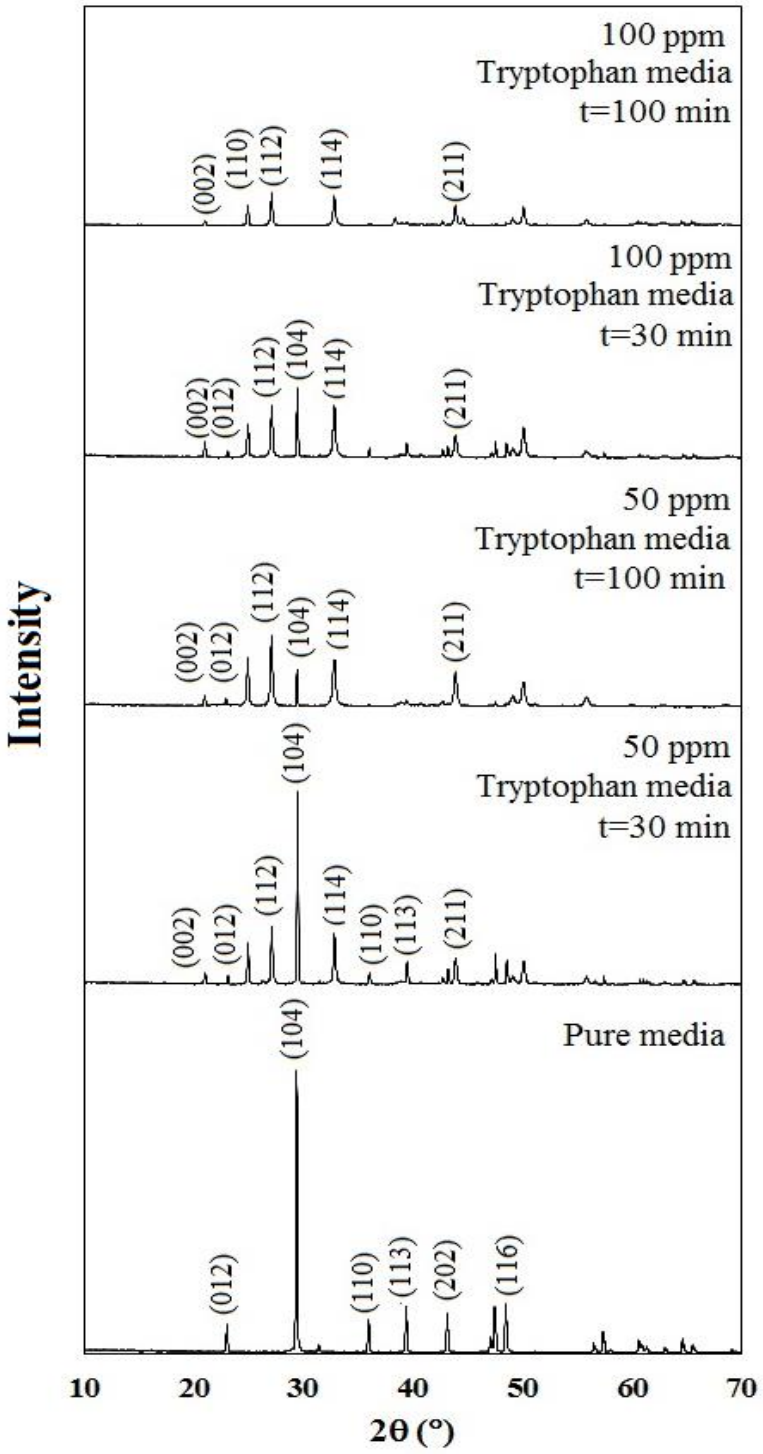

Figure 3.1. XRD results for $CaCO_3$ crystals precipitated in pure media and media supplemented with 50 and 100 ppm tryptophan.

3.1.2. FTIR Analysis

The FTIR spectra for $CaCO_3$ crystals precipitated with and without tryptophan at 30 and 100 min during the polymorphic phase transformation are presented in Figure 3.2.

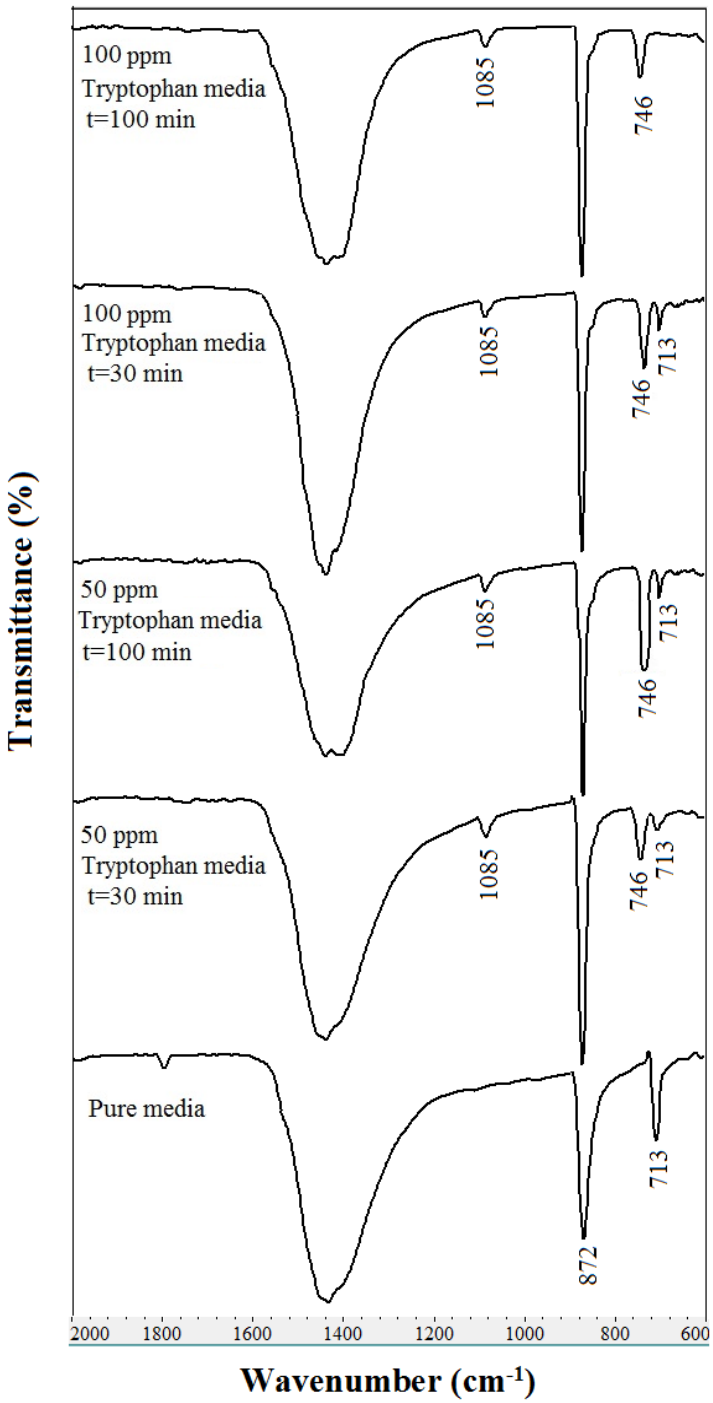

Figure 3.2. FTIR results for $CaCO_3$ crystals precipitated in pure media and media supplemented with 50 and 100 ppm tryptophan.

The calcite and vaterite absorption peaks are at different positions in the FTIR spectra. The absorption peak at 713 cm^{-1} is the characteristic peak of calcite, while the absorption peaks at 1085 cm^{-1} and 746 cm^{-1} correspond to vaterite [90]. The FTIR spectrum for the $CaCO_3$ crystals precipitated in pure media displayed the characteristic band of the calcite polymorph at 713 cm^{-1}. At t = 30 min, the two main characteristic peaks of vaterite were identified for the $CaCO_3$ crystals precipitated in the presence of 50 ppm tryptophan. Meanwhile, the intensity of the absorption peak at 713 cm^{-1} became obviously weaker. As the transformation progressed further, the intensity of the characteristic FTIR peaks of vaterite, especially that at 746 cm^{-1}, obviously increased while the intensity of the absorption peak at 713 cm^{-1} decreased. These FTIR results show the change of the crystal polymorphs from calcite only to a mixture of vaterite and calcite with a higher proportion of vaterite than calcite. With the higher tryptophan concentration, the intensity of the vaterite peak became stronger, while the corresponding peak of calcite became weaker. For the solid sample obtained at 100 min, the absorption peak at 713 cm^{-1} had completely disappeared in the FTIR spectrum and the sample mainly consisting of the vaterite polymorph and water, which was consistent with the XRD results.

3.1.3. SEM and AFM Analysis

The SEM image in Figure 3.3 shows that the surface of $CaCO_3$ crystals precipitated in pure media have smooth and non-porous crystal surfaces, and the crystals consist of regular cubic particles of almost the same size, which are consistent with the results of previous studies [91, 92].

Energy dispersive X-ray (EDX) spectroscopy was applied to determine the elemental composition of the $CaCO_3$ crystals. The EDX analysis showed a surface composition of Ca 40.12 wt%, C 11.97 wt%, and O 47.91 wt% for the crystals precipitated in pure media (Figure 3.4). The elemental content in $CaCO_3$ was thus consistent with the theoretical values. The average particle size and BET surface area of the $CaCO_3$ were 32 μm and 0.70 m^2/g, respectively. Based on the previous studies [93–96], $CaCO_3$ crystals precipitated without additive were generally characterized by small surface areas, below 1m^2/g, which was consistent with our result.

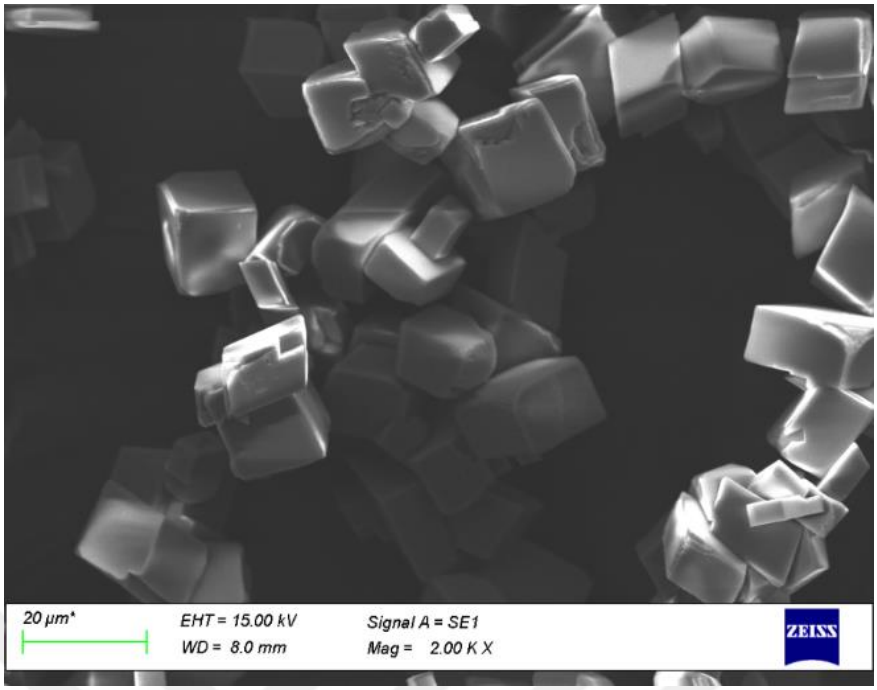

Figure 3.3. SEM images of $CaCO_3$ crystals precipitated in pure media.

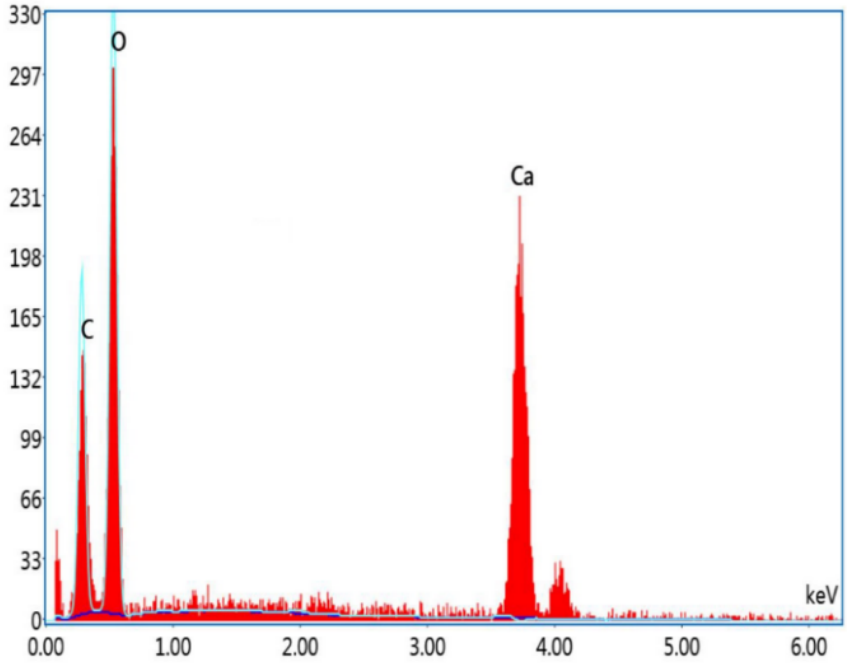

Figure 3.4. EDX results of $CaCO_3$ crystals precipitated in pure media.

The SEM images of the $CaCO_3$ crystals precipitated in the presence 50 and 100 ppm tryptophan at different time points are presented in Figure 3.5 and 3.6, respectively.

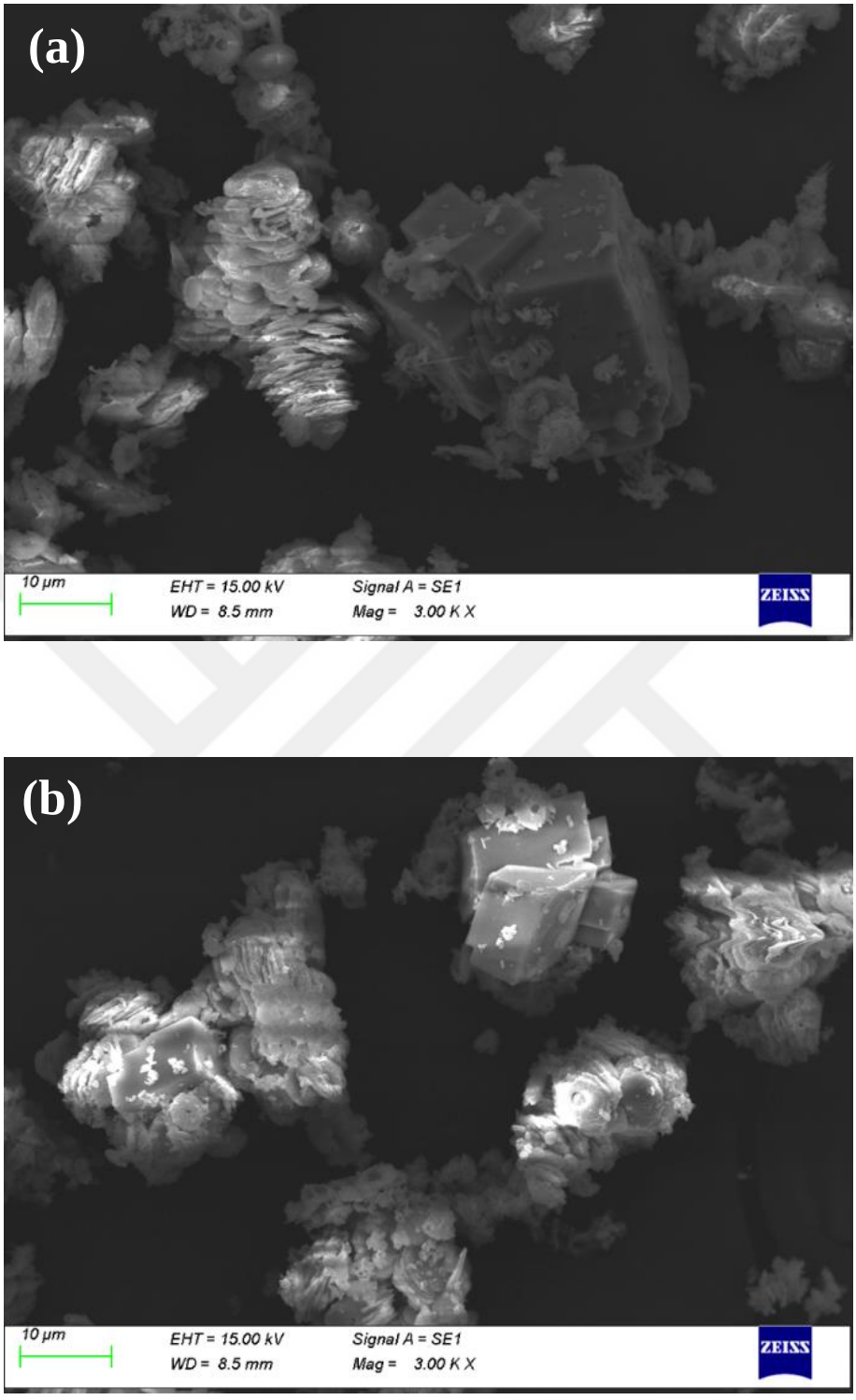

Figure 3.5. SEM images for $CaCO_3$ crystals precipitated with 50 ppm tryptophan at t = 30 min (a) and at t = 100 min (b).

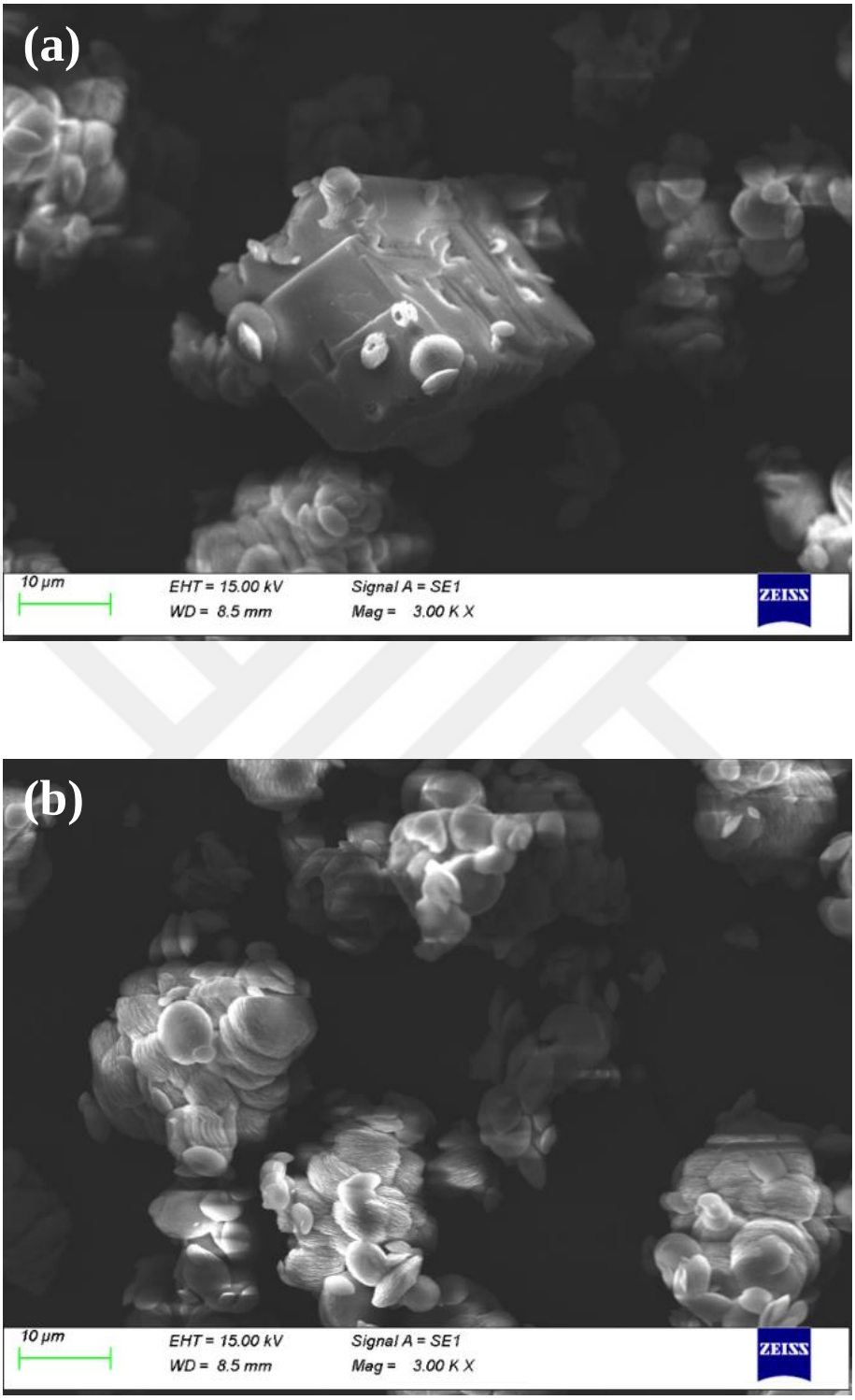

Figure 3.6. SEM images for $CaCO_3$ crystals precipitated with 100 ppm tryptophan at t = 30 min (a) and at t = 100 min (b).

At t = 30 min, in addition to cubic calcite crystals with an irregular surface, some small spherical shaped plate-like vaterite crystals were observed for 50 ppm additive media. That is, calcite and vaterite crystals were seen together, which was consistent with the XRD and FTIR results. With the increase of the transformation time to 100 min, the amount of cubic crystals decreased, surface deformations occurred on the calcite crystals, and some of the calcite was transformed to vaterite form. A similar outcome was also observed for crystals precipitated with 100 ppm tryptophan at 30 min. In addition to cubic calcite crystals, the sample also consisted of elliptical, intertwined, and compact agglomerates. These agglomerates took a spherical form owing to the effects of the hydrodynamic conditions of the media. At t = 30 min, both calcite and vaterite crystals were obtained. As the transformation process progressed, the cubic crystals disappeared completely and transformed into spherical-like vaterite crystals with an irregular crystal surface. With the completion of the transformation process, the obtained crystals had a spherical and ellipsoidal form, indicating that the calcite polymorph was completely converted into vaterite, which was also confirmed by the XRD and FTIR results. Meanwhile, the particle size and BET surface area of the samples precipitated in media supplemented with tryptophan were changed compared to the pure media due to the surface adsorption of the additive. The average particle sizes and BET surface areas of the samples precipitated in the presence of 50 and 100 ppm tryptophan were 26 μm and 3.8 m^2/g and 19 μm and 6.4 m^2/g, respectively. A higher additive concentration led to a decrease in the particle size and an increase in the specific surface area of the $CaCO_3$. Thus, more porous and rougher crystals with smaller sizes were produced in the presence of tryptophan.

To gain more insight into the effects of tryptophan on the topography of $CaCO_3$, AFM analysis was performed and 3D micrographs for the crystals precipitated with and without tryptophan are shown in Figure 3.7. The surface topography of the $CaCO_3$ crystals precipitated in pure media was flat and smooth with a maximum thickness of 31.17 nm. Compared to the crystals obtained in pure media, some ridges, defects, and irregularity occurred on the surface of $CaCO_3$ crystals precipitated in 100 ppm tryptophan media and the thickness increased to 117.45 nm. These changes led to increased surface roughness, confirming the results obtained from the SEM images.

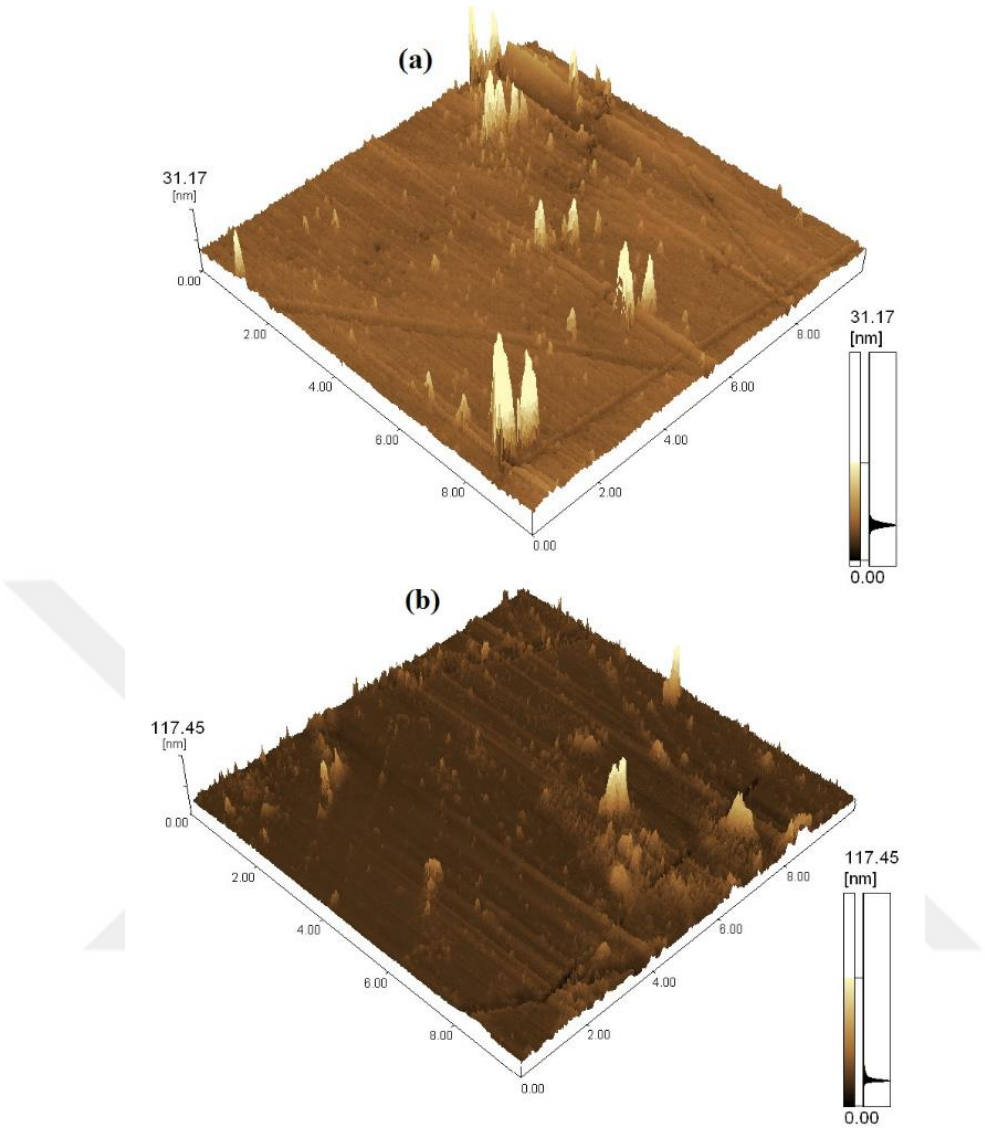

Figure 3.7. 3D micrographs for the crystals precipitated without (a) and with 100 ppm tryptophan (b).

3.1.4. Zeta Potential Analysis

The zeta potential of the $CaCO_3$ crystals precipitated with and without tryptophan in the media was investigated. The results are given in Figure 3.8. The $CaCO_3$ crystals prepared in pure media had a zeta potential of –8.1 ± 2.1 mV. Similar to pure media, the zeta potential of $CaCO_3$ crystals precipitated in additive media had a negative value. The zeta potential values at 50 ppm were -15.7 ± 1.0 mV, -17.4 ± 1.8 mV for t=30 and 100 mins, respectively.

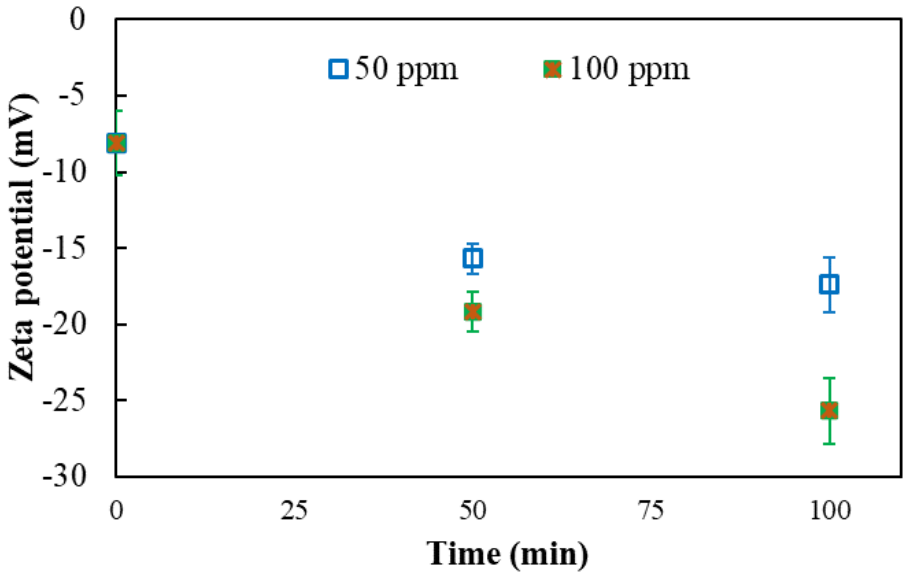

Figure 3.8. The change of zeta potential with time for tryptophan media.

As the tryptophan concentration increased, the zeta potential value of the $CaCO_3$ crystals showed a clear increase. The zeta potential values reached –19.2 ± 1.3 mV and –25.7 ± 2.2 mV at 100 ppm for t = 30 and 100 mins, respectively, which obviously illustrated that the electrical surface charge of the $CaCO_3$ crystals was more negative at a higher tryptophan concentration. This change in the zeta potential suggests that some tryptophan was adsorbed on the surface of $CaCO_3$ crystals.

3.1.5. Filtration Analysis

Filtration is an important parameter for controlling the precipitation of $CaCO_3$ since it affects both the properties of the crystalline products and process efficiency which is important from an economic point of view. In order to determine how tryptophan influences the filtration characteristics of $CaCO_3$, the average specific cake resistance and the average cake porosity of the crystals were analyzed based on Darcy's Law under 700 mbar constant pressure. The results are given in Table 3.1. The average specific cake resistance and the average cake porosity of the crystals precipitated in pure media were 1.03×10^{12} m/kg and 0.548, respectively.

Table 3.1. Filtration analysis results for tryptophan media.

Media	Concentration (ppm)	Specific cake resistance (m/kg)	Average cake porosity
Pure media	-	1.03×10^{12}	0.548
Tryptophan acid	50	9.65×10^{11}	0.658
	100	4.24×10^{11}	0.712

The filtration characteristics of the $CaCO_3$ are significantly changed by the addition of tryptophan to the media. Average specific cake resistances of 9.65×10^{11} m/kg and 4.24×10^{11} m/kg were obtained at the end of the polymorphic transformation process with tryptophan at 50 and 100 ppm, respectively. A higher concentration of tryptophan led to a lower specific cake resistance. Meanwhile, the average cake porosity increased from 0.658 to 0.712 as the tryptophan concentration increased from 50 to 100 ppm. This can be explained by the changes to the particle size, morphology, and polymorphic form, which have the greatest effect on these filtration characteristics. Fairly large differences in the sizes and shapes of the $CaCO_3$ crystals that were formed in the presence of tryptophan could be seen in the SEM images; these changes had a direct impact on the filtration properties. Therefore, appropriately increasing the tryptophan concentration could be advantageous for increasing the filtration rate and improving the filtration characteristics.

3.1.6. Thermogravimetric Analysis

The thermogravimetric (TG) and differential thermogravimetric (DTG) curves for the crystals precipitated in pure media and with 100 ppm tryptophan are presented in Figures 3.9 and 3.10, respectively.

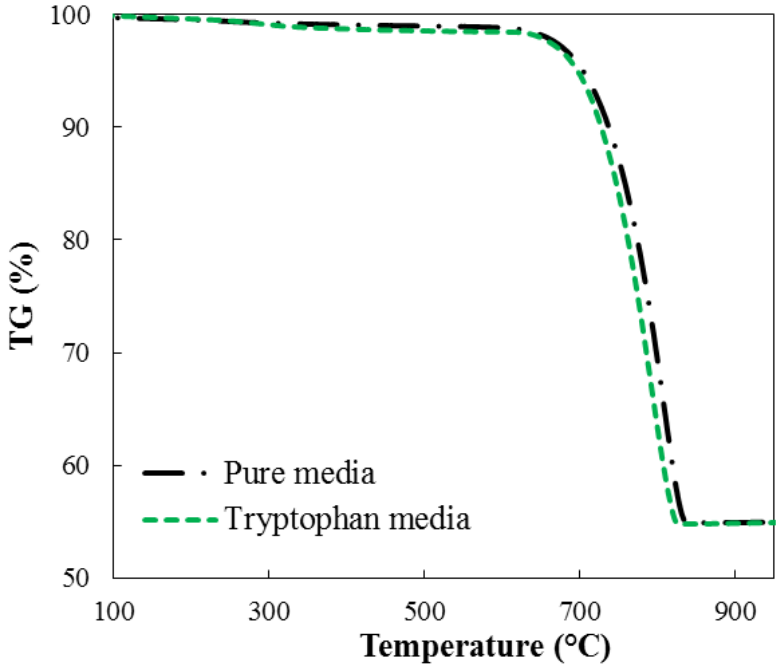

Figure 3.9. TG and DTG curves of $CaCO_3$ crystals precipitated in pure media.

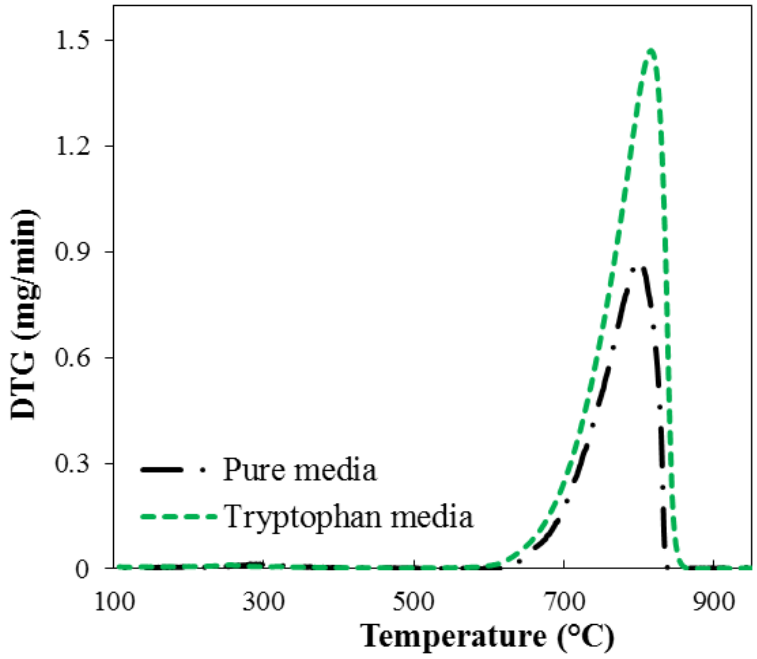

Figure 3.10. TG and DTG curves of $CaCO_3$ crystals precipitated with 100 ppm tryptophan.

Considering the thermal degradation characteristics of $CaCO_3$ crystals precipitated in pure media, a single DTG peak was observed, which showed that degradation occurred at a single stage, corresponding to the transformation of calcium carbonate to calcium oxide [97,98]. Thermal degradation occurred between 630 °C and 830 °C and the residual mass was 55.6 wt%, agreeing with the theoretical value. The weight loss from the $CaCO_3$ crystals precipitated in tryptophan media was 45.2 wt%. The higher weight loss suggests that tryptophan had been adsorbed onto and interacted with the surface of the $CaCO_3$ crystals. The addition of tryptophan had a significant effect on the temperature of the decomposition peak during the thermal decomposition of $CaCO_3$. Thus, adding tryptophan to the crystallization media shifted the decomposition peak to higher temperature.

3.1.7. Kinetic and Thermodynamic Analysis

In this study, the Coats–Redfern method was used to predict kinetic parameters such as activation energy and pre-exponential factor.

Coats–Redfern Method

The Coats–Redfern [99] model-fitting method is widely used for estimating the pre-exponential factor and activation energy to predict the order of a reaction. The basic equation for the Coats–Redfern method is as follows:

$$ln\left[\frac{g(\alpha)}{T^2}\right] = \ln\left[\frac{AR}{\beta E_a}\left(1-\frac{2RT}{E_a}\right)\right] - \frac{E_a}{RT} \quad (3.1)$$

where β is the heating rate, R is the ideal gas constant (8.314 J/mol K), and $g(\alpha)$ is a kinetic function of different reaction mechanisms that is obtained from integration of $f(\alpha)$. The activation energy (E) can be determined by plotting a graph of 1/T versus ln $[g(\alpha)/T^2]$ and determining the slope of the straight line of best fit. The intercept of the line gives the pre-exponential factor (A) and g(α) varies depending on the developed model and reaction mechanism. Most solid-state degradation reactions fall into one of five main categories, as detailed in Table 3.2 [100,101].

Table 3.2. Reaction mechanisms and symbols with their f(α) and g(α).

Mechanisms	Symbol	f(α)	g(α)
Reaction order			
First-order	F_1	$(1-\alpha)$	$-\ln(1-\alpha)$
Second-order	F_2	$(1-\alpha)^2$	$(1-\alpha)^{-1}-1$
One and half order	$F_{1.5}$	$(1-\alpha)^{3/2}$	$2[(1-\alpha)^{-1/2}-1]$
Diffusion phenomena			
Parabolic Law	D_1	0.5α	α^2
Valensi equation	D_2	$[-\ln(1-\alpha)]^{-1}$	$\alpha+(1-\alpha)\ln(1-\alpha)$
Phase interfacial reaction			
Shrinkage geometrical column	R_2	$2(1-\alpha)^{1/2}$	$1-(1-\alpha)^{1/2}$
Shrinkage geometrical spherical	R_3	$3(1-\alpha)^{2/3}$	$1-(1-\alpha)^{1/3}$
Exponential nucleation			
Power law, n = 1/2	P_2	$2\alpha^{1/2}$	$\alpha^{1/2}$
Power law, n = 1/3	P_3	$3\alpha^{2/3}$	$\alpha^{1/3}$
Nucleation and growth			
Avrami-Erofeev two dimensional	A_2	$2(1-\alpha)[-\ln(1-\alpha)]^{1/2}$	$[-\ln(1-\alpha)]^{1/2}$
Avrami-Erofeev three dimensional	A_3	$3(1-\alpha)[-\ln(1-\alpha)]^{1/3}$	$[-\ln(1-\alpha)]^{1/3}$

Thermodynamic analysis

The thermodynamic parameters of the $CaCO_3$ crystals, including change in enthalpy (ΔH), change in Gibbs free energy (ΔG), and change in entropy (ΔS), were calculated based on kinetic data from the following equations [102]

$$\Delta H = E_\alpha - RT \tag{3.2}$$

$$\Delta G = E_\alpha + RT_{peak} \ln\left(\frac{K_B T_{peak}}{hA}\right) \tag{3.3}$$

$$\Delta S = \frac{\Delta H - T\Delta G}{T_{peak}} \tag{3.4}$$

Where T_{peak} is the peak temperature of DTG curve, K_B is the Boltzmann constant, and h is the Planck constant.

The minimum energy required to initiate a reaction, known as the activation energy, can be determined by kinetic analysis. As shown in Table 3.3, the activation energies were between 56.6 and 442.6 kJ/mol, which was consistent with the results of previous studies [103,104]. The pre-exponential factors were in the range of 3.08×10^1 to 6.11×10^{20} min^{-1}, in good agreement with the literature [104].

Linear adjustment using the different reaction mechanisms as shown in Table 3.1 was applied to estimate the reaction mechanism for the thermal degradation of $CaCO_3$. It was found from Table 3.2 that the thermal degradation of $CaCO_3$ predicted by the geometric spherical shrinkage mechanism (the R_3 type model) fitted the experimental data best, which was consistent with previous research [103,104]. The regression coefficients ranged between 0.9630 and 0.9954 depending on the applied kinetic model. The R_3 type model presented the highest accuracy ($R^2 = 0.9954$) of the 11 models studied.

The thermodynamic parameters of enthalpy (ΔH), entropy (ΔS), and Gibbs free energy (ΔG) for the thermal decomposition of $CaCO_3$ were calculated using different reaction mechanism models. According to the thermodynamic results presented in Table 3.3, the enthalpy change for the thermal decomposition of $CaCO_3$ was between 47.6 and 433.6 kJ/mol depending on the model used. Diffusion models D1 and D2 gave higher ΔH values that the other models tested, including the reaction, interfacial, exponential, nucleation, and growth models. Obtaining positive ΔH values for the crystals affirmed that the main decomposition process took place endothermic in nature. The entropy changes for the crystals were in the range of −235.8 to 133.6 J/mol K. The Gibbs free energy change was calculated to be between 233.0 and 302.9 kJ/mol. A positive value of ΔG indicates that a reaction is unfavorable and thus energy needs to be supplied for the reaction to occur.

Table 3.3. Kinetic calculation results for thermal decomposition of $CaCO_3$ using the Coats–Redfern method.

Symbol	E_a (kJ/mol)	A (min^{-1})	R^2	ΔH (kJ/mol)	ΔG (kJ/mol)	ΔS (J/mol.K)
F_1	242.8	1.86×10^{11}	0.9891	233.8	286.4	–48.6
F_2	281.0	3.09×10^{13}	0.9813	272.0	278.6	–6.09
$F_{1.5}$	257.8	1.53×10^{12}	0.9908	248.8	282.4	–31.1
D_1	423.1	9.98×101^{9}	0.9772	414.1	285.8	118.5
D_2	442.6	6.11×10^{20}	0.9842	433.6	289.0	133.6
R_2	218.9	4.87×10^{9}	0.9865	209.9	295.3	–78.9
R_3	**224.6**	**6.88×10^{9}**	**0.9954**	**215.6**	**297.9**	**–76.0**
P_2	93.3	4.27×10^{6}	0.9698	84.3	233.0	–137.4
P_3	56.6	3.08×10^{1}	0.9630	47.6	302.9	–235.8
A_2	110.1	2.93×10^{4}	0.9892	101.2	294.7	–178.8
A_3	69.8	1.98×10^{2}	0.9850	60.8	299.4	–220.4

3.1.8. Experiment Design Results

Response surface methodology (RSM) is a multivariate statistical technique that is used to optimize process variables and their responses by exploring the relationship between independent process variables and their observed responses. Box–Behnken design, central composite design (CCD), and three-level factorial design are examples of experimental design techniques. In this study, Design Expert software version 10 (Stat-Ease, Minneapolis, USA) was used for the experimental design using CCD [37]. We conducted 17 experiments with three center points using three variables of temperature (A), stirring rate (B), and tryptophan concentration (C), and the vaterite content was chosen as the response. Meanwhile, CCD with three factors and five levels was also applied to determine the correlation between the combined effects of individual variables.

Table 3.4. Experimental variables and their levels in central composite design matrix.

Parameters	Factors	Levels				
		-2	-1	0	+1	+2
Temperature (°C)	A	20	25	30	35	40
Stirring rate (rpm)	B	400	450	500	550	600
Tryptophan concentration	C	0	25	50	75	100

Table 3.5. Central composite design matrix and results.

Run	Actual level of factors			Coded level of factors			Response
	Temperature (°C)	Stirring rate (rpm)	Concentration (ppm)	A	B	C	Vaterite composition
1	25	450	25	-1	-1	-1	19.2
2	35	450	25	+1	-1	-1	27.2
3	25	550	25	-1	+1	-1	25.4
4	35	550	25	+1	+1	-1	31.6
5	25	450	75	-1	-1	+1	60.6
6	35	450	75	+1	-1	+1	70.3
7	25	550	75	-1	+1	+1	64.4
8	35	550	75	+1	+1	+1	75.9
9	20	500	50	-2	0	0	34.7
10	40	500	50	+2	0	0	44.4
11	30	400	50	0	-2	0	40.6
12	30	600	50	0	+2	0	51.8
13	30	500	0	0	0	-2	0
14	30	500	100	0	0	+2	100
15	30	500	50	0	0	0	41.8
16	30	500	50	0	0	0	42.4
17	30	500	50	0	0	0	41.0

Tables 3.4 and 3.5 show the range and levels, respectively, of the investigated variables and their responses for all 17 optimized test experimental runs. Thus, based on these results, the model equation for the vaterite content as a function of the process variables is:

$$Y = 42.59 + 3.42A + 2.65B + 22.99C + 0.87AC - 0.15BC - 0.44A^2 + 1.22B^2 + 2.17C^2 \quad (3.5)$$

The lowest vaterite composition (19.2%) was obtained at 25 °C, 450 rpm, and 50 ppm tryptophan concentration (apart from the sample obtained in pure media at 30 °C and 500 rpm).

The model and factor significances with respect to vaterite content were examined by variance analysis (ANOVA) of the F test and p-values. The results are shown in Table 3.6. The obtained values of F and p suggest that the experimental values are significant and thus acceptable. The ANOVA results showed a large F of 63.59 and a small *p*-value << 0.0001, which verified that the model fit was statistically significant. The obtained correlation coefficient (R^2) of 0.9879 showed that there was good correlation between the measured and predicted responses and confirmed that the model was suitable for the experimental data. The CCD analysis shows that the three independent process variables played an important role in determining the amounts of the $CaCO_3$ polymorphs formed since its p-value was <0.05 and had positive coefficients.

Increasing the temperature, stirring rate, and tryptophan concentration increased the amount of vaterite formed and they were thus significant and favorable factors. However, the strength and significance of the effect varied for each parameter. The p-value of <0.0001 for tryptophan concentration shows that it is the most important variable to control. However, the interaction of tryptophan concentration with other parameters had a less significant effect. Thus, this establishes tryptophan concentration as the most influential parameter during the polymorphic transformation of $CaCO_3$.

The effects of the independent variables and their interactions are presented in the three-dimensional (3D) response surface plots and contour plots in Figure 3.11. According to the results, the 3D surface plots are flat with the slope being related to linear terms of the variables. As shown in Figure 3.11, when more than one factor is changed at a time,

different effects on the response are observed. The highest vaterite content was obtained with the highest additive concentration, temperature, and stirring rate. In comparison with temperature and stirring rate, tryptophan concentration had the most significant effect on the amount of vaterite produced.

Table 3.6. ANOVA results of the quadratic model for vaterite content.

Source	Sum of Squares	df	Mean Square	F-Value	p-value Prob > F
Model	8904.63	9	989.40	63.59	< 0.0001
A-Temperature	187.69	1	187.69	12.06	0.0104
B-Stirring rate	112.36	1	112.36	7.22	0.0312
C-Tryptophan concentration	8454.80	1	8454.80	543.43	< 0.0001
AB	0.000	1	0.000	0.000	1.0000
AC	6.13	1	6.13	0.39	0.5503
BC	0.18	1	0.18	0.012	0.9174
A^2	3.73	1	3.73	0.24	0.6391
B^2	28.99	1	28.99	1.86	0.2145
C^2	91.49	1	91.49	5.88	0.0458
Residual	108.91	7	15.56		
Lack of Fit	107.92	5	21.58	43.75	0.0225
R^2	0.9879				

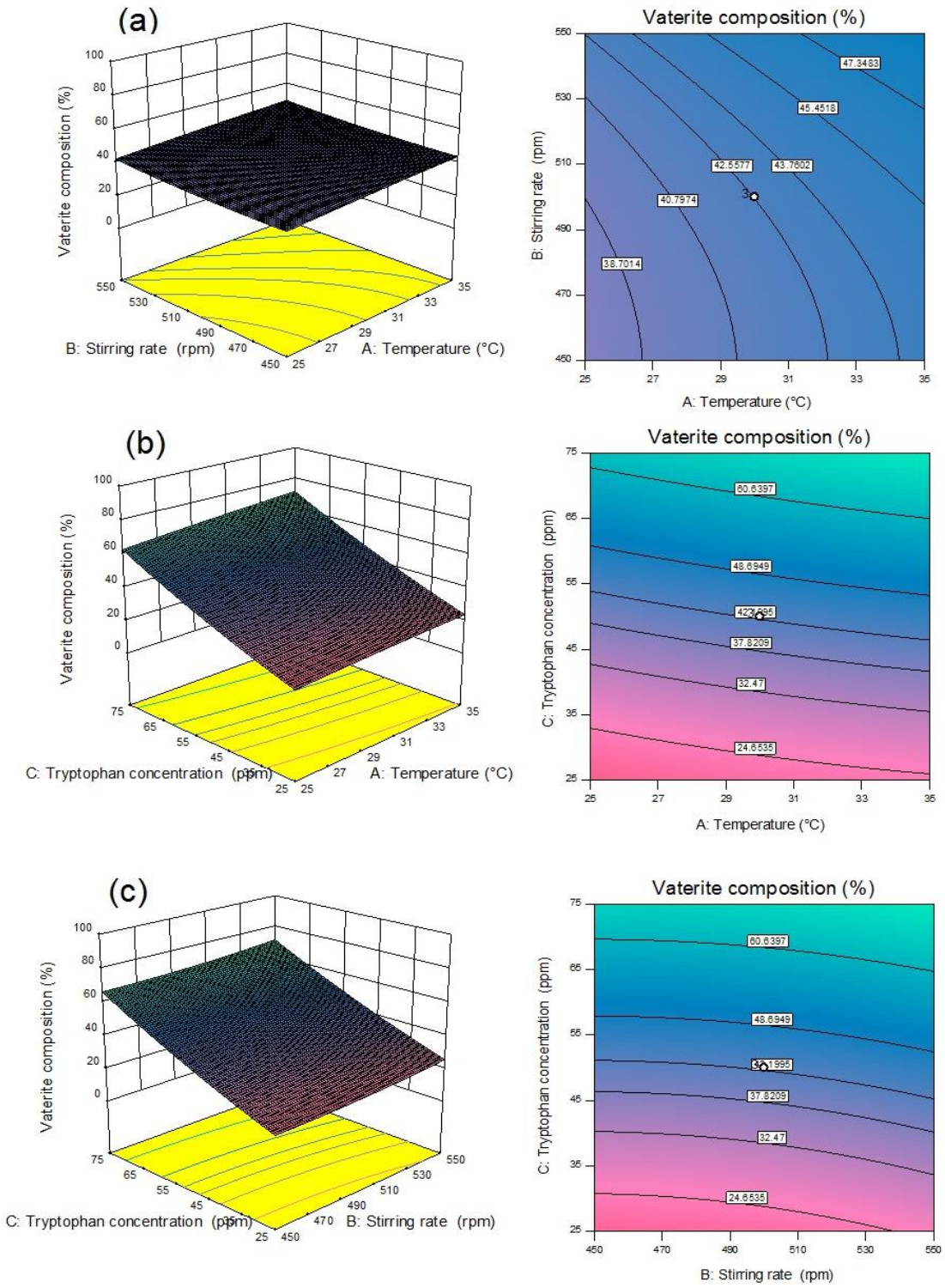

Figure 3.11. 3D-surface and contour plots showing the effects of (a) temperature and stirring rate; (b) temperature and tryptophan concentration; and (c) stirring rate and tryptophan concentration on the vaterite composition.

3.2. The Results of Effects of Glutamic Acid on the Polymorphic Transformation of Calcium Carbonate•

3.2.1. XRD Analysis

Figure 3.12 illustrates the XRD patterns of $CaCO_3$ crystals with and without glutamic acid in which C represents peaks from calcite, while V denotes peaks from vaterite within the range of 10–70°.

XRD results for the crystals acquired in pure media showed that calcite was the only major crystallization product. All the main characteristic peaks of the crystal products with corresponding faces (012), (104), (110), (113) and (022) were the standard pattern of calcite form (JCPDS: 05-0586). The addition of glutamic acid to the solution led to significant changes in crystal structure and new crystallization products were formed. In addition to the characteristic diffraction peaks of calcite, the new diffraction peaks of vaterite were detected at 2θ = 21.0°, 24.9°, 27.1°, 32.7°, and 50.1° (JCPDS: 33-0268). For the solid sample obtained at 30 min, the characteristics peaks of both calcite and vaterite were seen together. As time goes by, the characteristic peak intensity of vaterite enhanced, while that of the calcite weaken. At t=100 min, the calcite peaks disappeared completely and the vaterite was the only crystallization product at each characteristic point of the system. The XRD results showed that glutamic acid altered the crystal form of $CaCO_3$.

3.2.2. FTIR Analysis

The calcite and vaterite polymorphs could be distinguished according to FTIR Spectra. The spectra of calcite and vaterite are obviously different. Thus, except for XRD analysis, FTIR analysis was performed to follow the polymorphic phase transformation of $CaCO_3$. The FTIR spectra for $CaCO_3$ crystals with and without glutamic acid are given in Figure 3.13.

• Polat, S., Ozalp, T.N., Sayan P. (2021) Polymorphic Phase Change of Calcium Carbonate with Glutamic Acid as an Additive, Journal of the Turkish Chemical Society Section A: Chemistry, 8(1), 117-124.

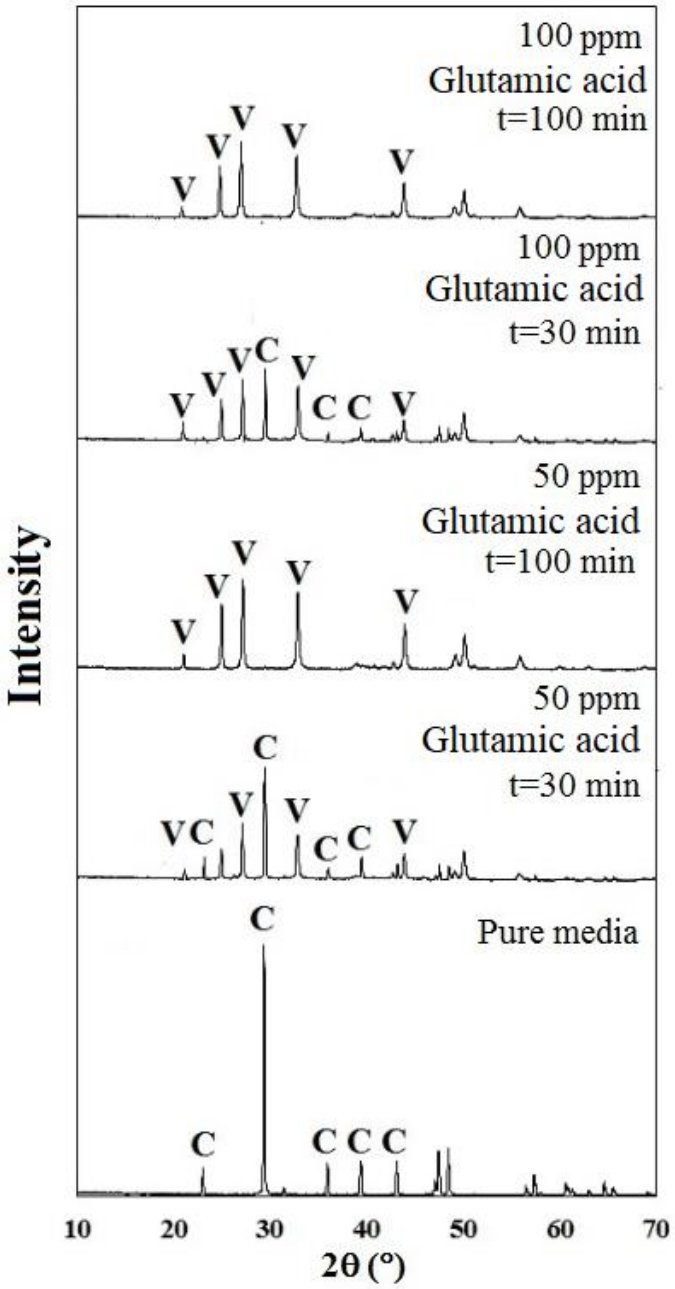

Figure 3.12. XRD results for $CaCO_3$ crystals precipitated in pure media and media supplemented with 50 and 100 ppm glutamic acid.

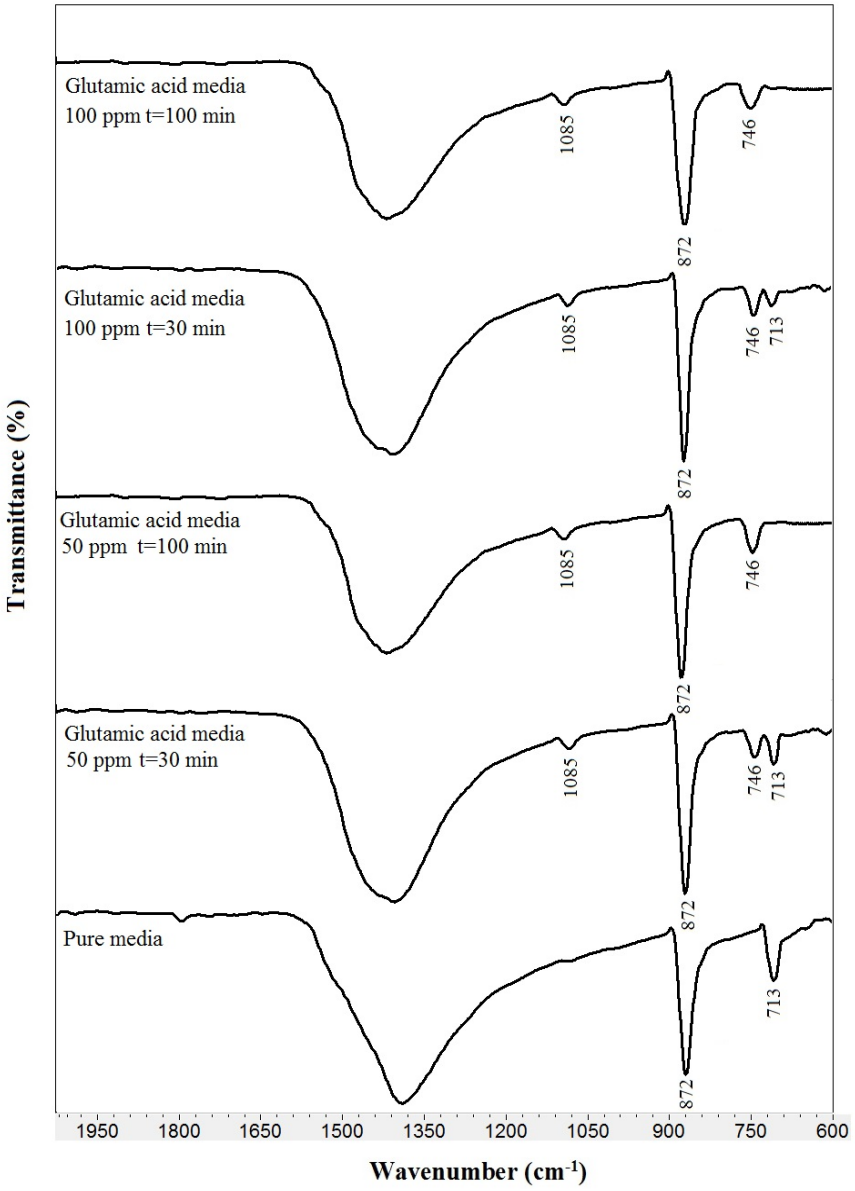

Figure 3.13. FTIR results for $CaCO_3$ crystals precipitated in pure media and media supplemented with 50 and 100 ppm glutamic acid.

The FTIR spectrum of the $CaCO_3$ crystals acquired in pure media is very similar in the intensity and position of the main characteristic absorption peak (712 cm^{-1}) with that of calcite form reported by the previous studies [105,106]. When the FTIR spectra for the crystals with 50 and 100 ppm glutamic acid at 30 min were examined, new additional absorption bands not in the spectrum of the crystals acquired in pure media were detected at 1085 cm^{-1} and 746 cm^{-1} belonged to the vaterite polymorph. The crystal products acquired in the presence of 50 ppm additive concentration were mixtures of calcite and

vaterite, and the intensity of the calcite peaks was weaker than the intensity of the vaterite peaks. At higher additive concentration, intensity of the peaks of the calcite was very weak while the corresponding main absorption peak of vaterite was very strong. FTIR spectra for the crystals acquired at t=100 min showed that the crystal products were all vaterite purely. These results are supported by the XRD patterns.

3.2.3. SEM Analysis

SEM analysis was conducted to explore the effect of glutamic acid and its concentration on the surface character of $CaCO_3$ crystals. As mentioned above, the $CaCO_3$ crystals acquired in pure media consisted mainly of smooth and uniform cubic calcite crystals with the mean particle size of 32.0 μm as shown in Figure 3.3. As can be seen from Figures 3.14 and 3.15, the morphological characteristics of the $CaCO_3$ crystals were directly related to the transformation time and glutamic acid concentration. Examining the SEM image of the crystals with 50 ppm glutamic acid at 30 min (Figure 3.14a), the cubic calcite crystals started to change. Alongside the cubic calcite crystals, vaterite crystals with a round appearance started to form. The formed crystals consisted of highly robust agglomerates. As the transformation process continued, the cubic calcite crystals were no longer formed, and all of the crystals were spherical-like vaterite crystals with the rough surface aggregated by many particles (Figure 3.14b). Moreover, there was a significant increment in the counts of small particles. When the SEM image of the crystal products acquired with 100 ppm additive at 30 min (Figure 3.15a) was examined, it was determined that there was more transformation of calcite into vaterite crystals in comparison to the concentration of 50 ppm. However, the two polymorphs were still found together in the same medium, and the obtained crystals had an irregular shape, and some of the crystals formed irregular aggregates. The vaterite crystals grown on the surfaces of the untransformed calcite crystals were in an ellipsoidal form with a plate structure. As the transformation process progressed, the calcite crystals completely transformed to the vaterite and gained a spherical and ellipsoidal appearance (Figure 3.15b). The surface of the crystals was rough and included a lot of spherical-like particles aggregated. It was also detected that the mean particle size of the final products was smaller in comparison to both pure and 50 ppm additive media.

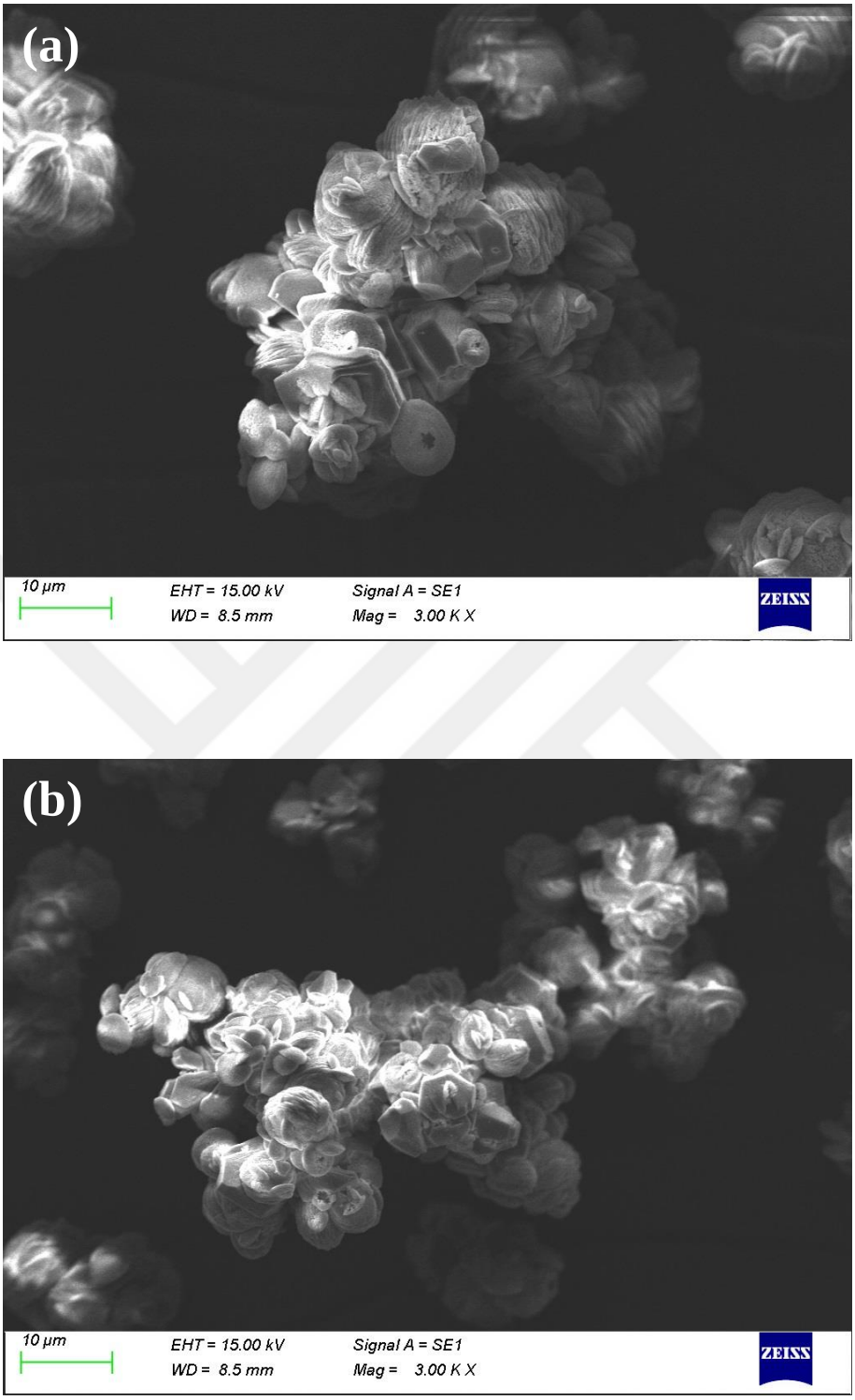

Figure 3.14. SEM images for $CaCO_3$ crystals acquired media supplemented with 50 ppm glutamic acid at t = 30 min (a) and at t = 100 min (b).

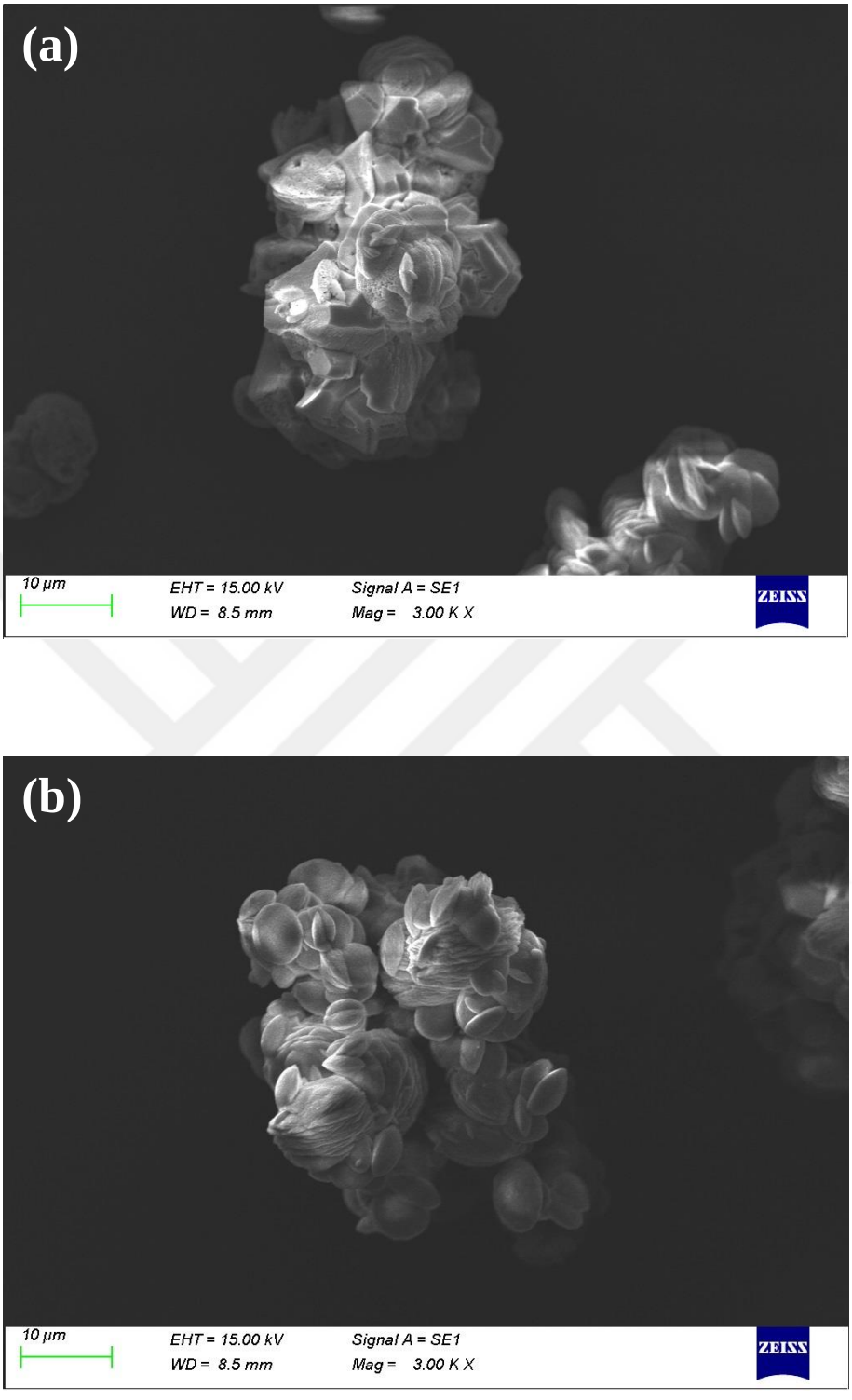

Figure 3.15. SEM images for $CaCO_3$ crystals acquired media supplemented with 100 ppm glutamic acid at t = 30 min (a) and at t = 100 min (b).

As shown in Figure 3.16, the mean particle size of $CaCO_3$ decreased from 17.9 to 14.6 μm as the glutamic acid concentration increased from 50 to 100 ppm. It can be concluded that the glutamic acid had a profound effect on the controlling the polymorph, habit, and particle size of the crystals due to its adsorption on the active site of $CaCO_3$.

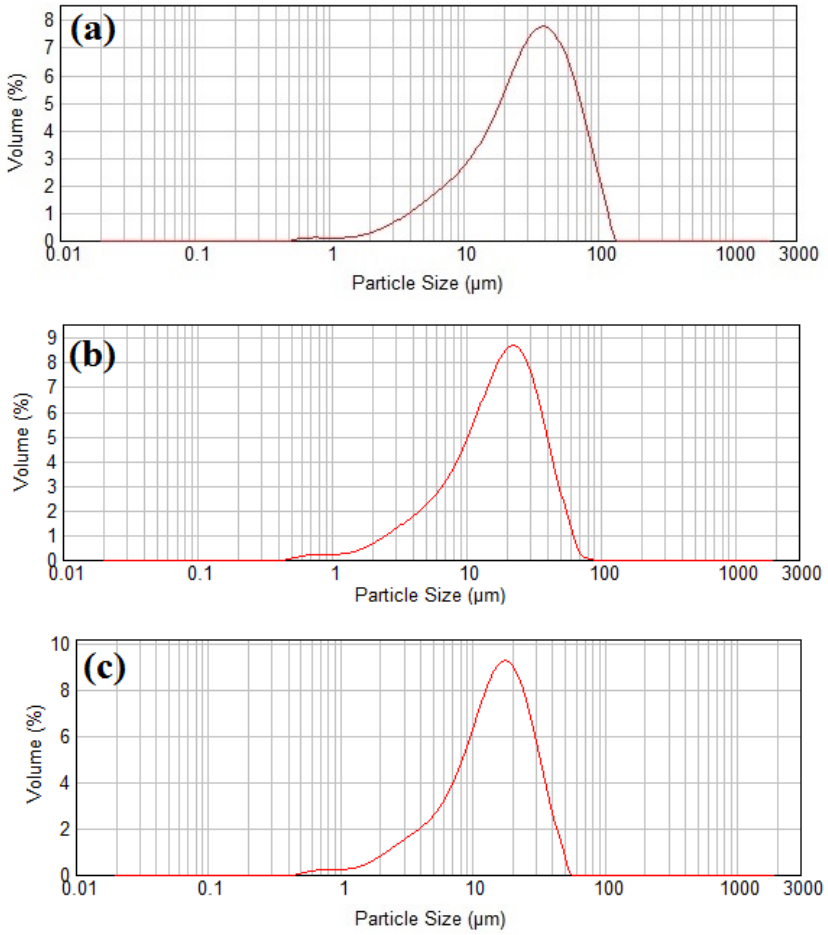

Figure 3.16. Particle size distributions for $CaCO_3$ crystals acquired in pure media (a) and media supplemented with 50 ppm glutamic acid (b) and with 100 ppm glutamic acid (c).

3.2.4. Zeta Potential Analysis

The zeta potential of the $CaCO_3$ crystals with and without glutamic acid was investigated to determine the surface charge of the samples. The results are given in Figure 3.17. As mentioned above, the zeta potential of $CaCO_3$ crystals acquired in pure media was –8.1 ± 2.1 mV.

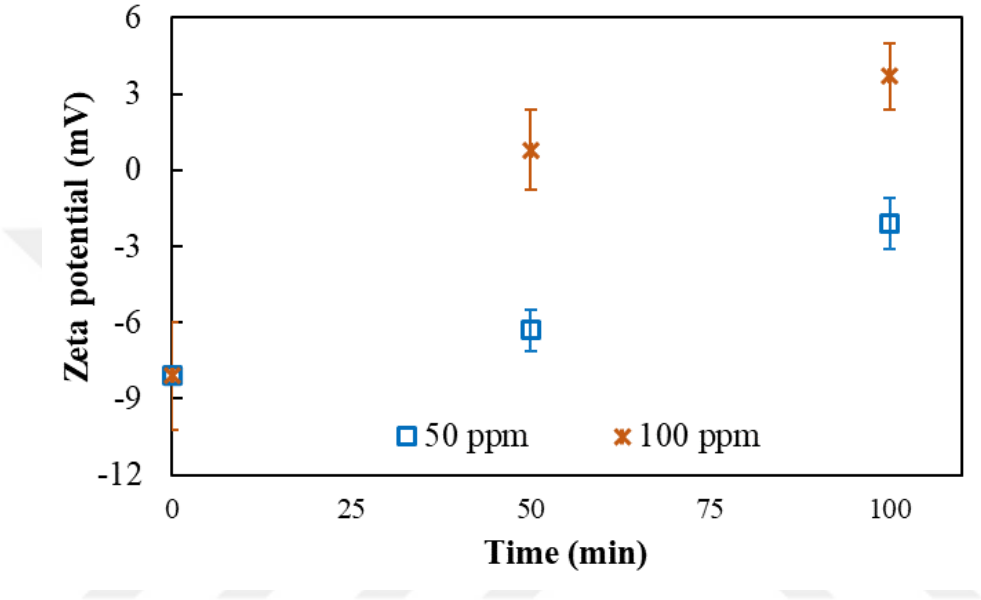

Figure 3.17. The change of zeta potential with time for glutamic acid media.

The addition of glutamic acid to the crystallization media led to a distinctive change in surface charge and the zeta potential value at 50 ppm reached –6.3 ± 0.8 mV and –2.1 ± 1.0 mV for t=30 and 100 mins, respectively. The zeta potential value of $CaCO_3$ crystals acquired in 100 ppm additive media showed a rising tendency and the electrical surface charge was more positive.

3.2.5. Filtration Analysis

Filtration characteristics of $CaCO_3$ is important for economic considerations since this characteristic is closely related with energy consumption during the filtration process. Therefore, the filtration property of the $CaCO_3$ crystals with and without additive was evaluated by Darcy's Law under 700 mbar constant pressure. The results are shown in Table 3.7. As mentioned above, the average specific cake resistance and the average cake

porosity of the $CaCO_3$ crystals acquired without glutamic acid were 1.03×10^{12} m/kg and 0.548, respectively.

Table 3.7. Filtration analysis results for glutamic acid media.

Media	**Concentration (ppm)**	**Specific cake resistance (m/kg)**	**Average cake porosity**
Pure media	-	1.03×10^{12}	0.548
Glutamic acid	50	8.26×10^{11}	0.589
	100	5.01×10^{11}	0.703

When 50 ppm glutamic acid was added to the crystallization media, the average specific cake resistance decreased to 8.26×10^{11} m/kg. Increasing the additive concentration to 100 ppm caused to significantly reduce the effect on the specific cake resistance (5.01×10^{11} m/kg). In the same time, the average cake porosity increased from 0.589 to 0.703 as the glutamic acid concentration increased from 50 to 100 ppm due to the change of the crystal size and habit.

3.3. The Results of Effects of Threonine on the Polymorphic Transformation of Calcium Carbonate•

3.3.1. XRD Analysis

Polymorphic phase transformation of $CaCO_3$ acquired in the presence of threonine was monitored by XRD analysis. Figure 3.18 shows the XRD results of samples taken in different additive concentrations depending on time. As mentioned above, $CaCO_3$ crystals obtained in pure media were in calcite form. $CaCO_3$ crystals acquired at t=30 min in the presence of 50 ppm threonine included the form of vaterite as well as the calcite polymorphs. In particular, the new peaks appeared at $2\theta = 24.9°$, 27.1°, and 32.7° were the characteristic peaks of the vaterite form. In other words, a partial phase transformation from calcite to vaterite form took place in the presence 50 ppm threonine at t=30 min. As time progressed (t=100 min), all peaks characterizing the calcite polymorph were completely lost. All obtained crystals were in the form of vaterite. A similar result was also valid for 100 ppm threonine concentration. Unlike 50 ppm concentration, more vaterite formation was observed at t=30 min for 100 ppm concentration. This was clearly observed from the change in the intensity of calcite and vaterite peaks. At t=100 min, calcite peaks completely disappeared and full phase transformation took place. As a result, $CaCO_3$ crystals at both low and high threonine concentrations tended to transform from calcite form to vaterite form.

3.3.2. FTIR Analysis

In parallel with the XRD analysis, FTIR analysis was performed both to monitor phase transformation and to detect functional groups of $CaCO_3$ crystals. FTIR analysis results are illustrated in Figure 3.19. $CaCO_3$ crystals precipitated in pure media were in calcite structure as stated in the XRD analysis. In particular, the peak detected at 713 cm^{-1} was the characteristic peak of calcite polymorph.

• Presented by Ozalp, T.N., Polat, S., Sayan P. International Eurasian Conference on Biotechnology and Biochemistry (BioTechBioChem 2020).

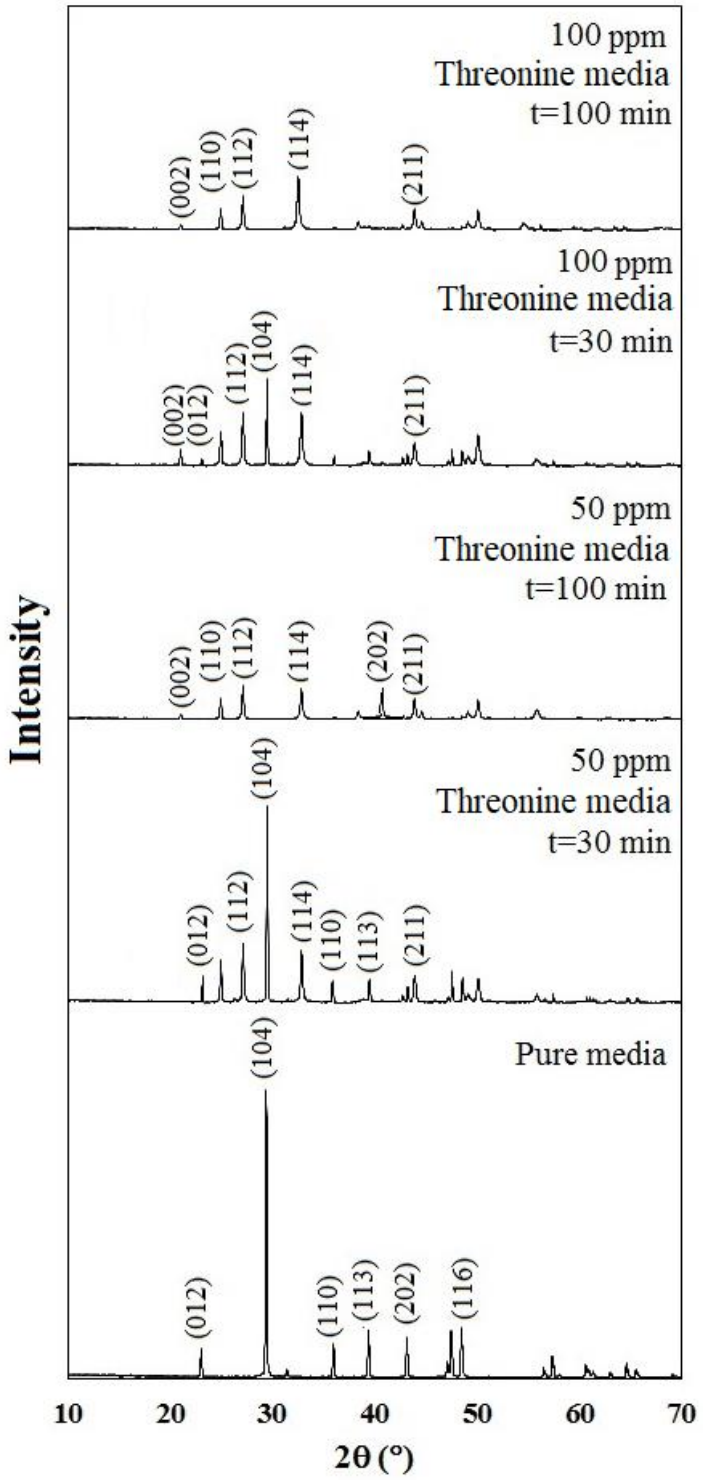

Figure 3.18. XRD results for $CaCO_3$ crystals precipitated in pure media and media supplemented with 50 and 100 ppm threonine.

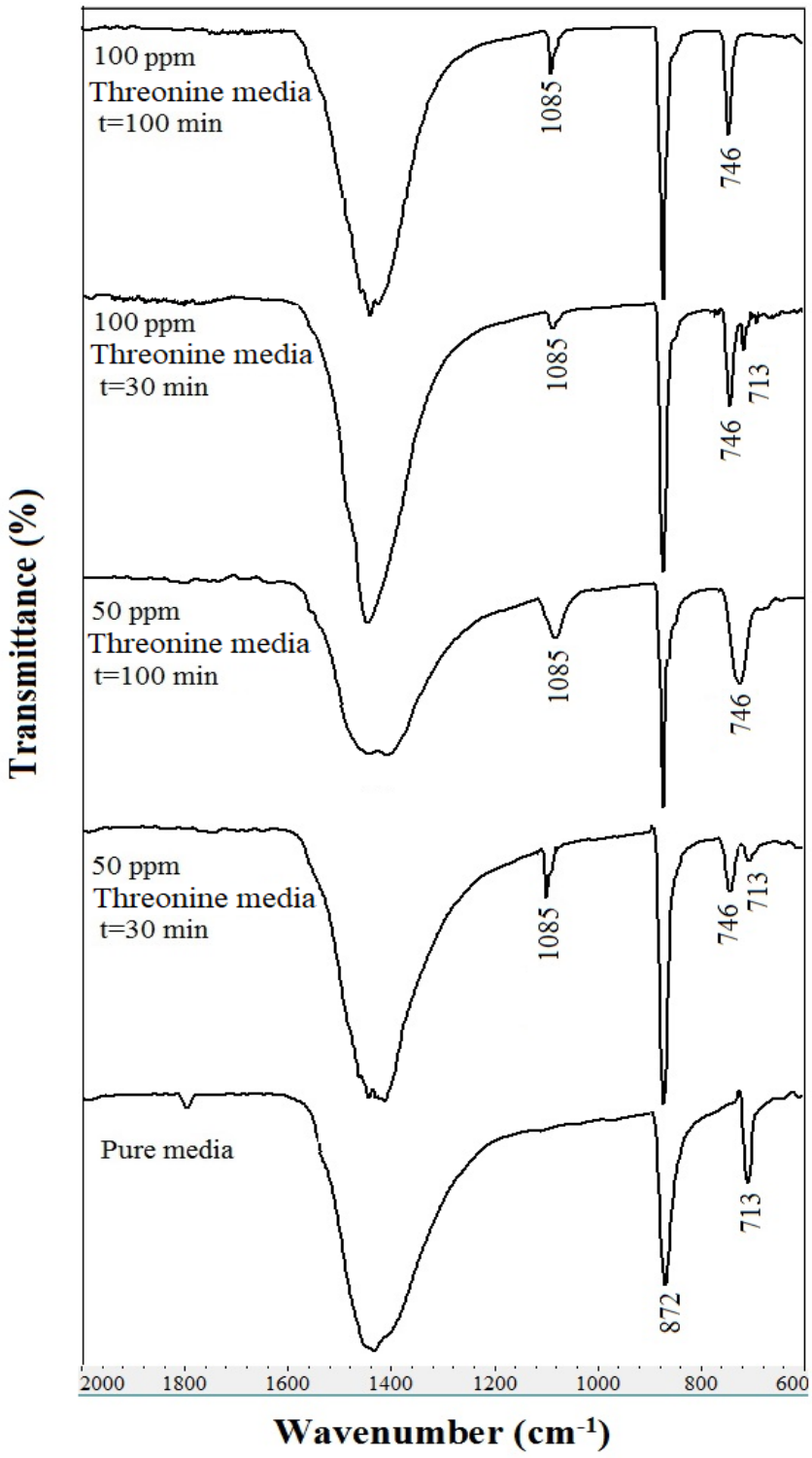

Figure 3.19. FTIR results for $CaCO_3$ crystals precipitated in pure media and media supplemented with 50 and 100 ppm threonine.

New peaks as well as characteristic calcite peaks were detected by adding 50 ppm threonine to the crystallization medium. These peaks detected at 1085 cm^{-1} and 746 cm^{-1} characterized the vaterite polymorph. In other words, both calcite and vaterite polymorph were found together. Calcite peaks were completely replaced by vaterite peaks at a concentration of 50 ppm at t=100 min. Similar results were also observed for 100 ppm additive concentration. At t =30 min calcite and vaterite polymorph were found, while only vaterite form was obtained at t=100 min. FTIR and XRD results are supported each other.

3.3.3. SEM Analysis

In this study, the polymorphic transformation of $CaCO_3$ crystals from calcite to vaterite polymorph was examined both structurally and morphologically. SEM analysis of the crystals was conducted to observe morphological change and the results are given in Figures 3.20 and 3.21.

As mentioned before, calcite crystals were in cubic form and were properly constructed. When Figure 3.20 was examined, deformations occurred on the surfaces of cubic calcite crystals at t=30 min for 50 ppm threonine concentration. In addition, there were new crystal formations on these surfaces. These new crystals were vaterite forms, as proven by XRD and FTIR analysis. With passing the time, cubic calcite crystals were replaced the round surfaces with porous vaterite crystals. Furthermore, the surfaces of the crystals were quite different in comparison with the pure medium. The precipitated crystals tended to grow on one another. When SEM images of crystals precipitated at 100 ppm threonine concentration were examined, round-structured vaterite crystals and mostly cubic calcite crystals were found together at t=30 min. As a result of the precipitation process, all cubic forms were transformed into round structures. In addition, the average particle sizes of the crystals decreased according to both pure and 50 ppm additive concentration. As a result, cubic crystals were replaced by round shaped crystals. The threonine used as the additives caused significant changes in crystal morphology.

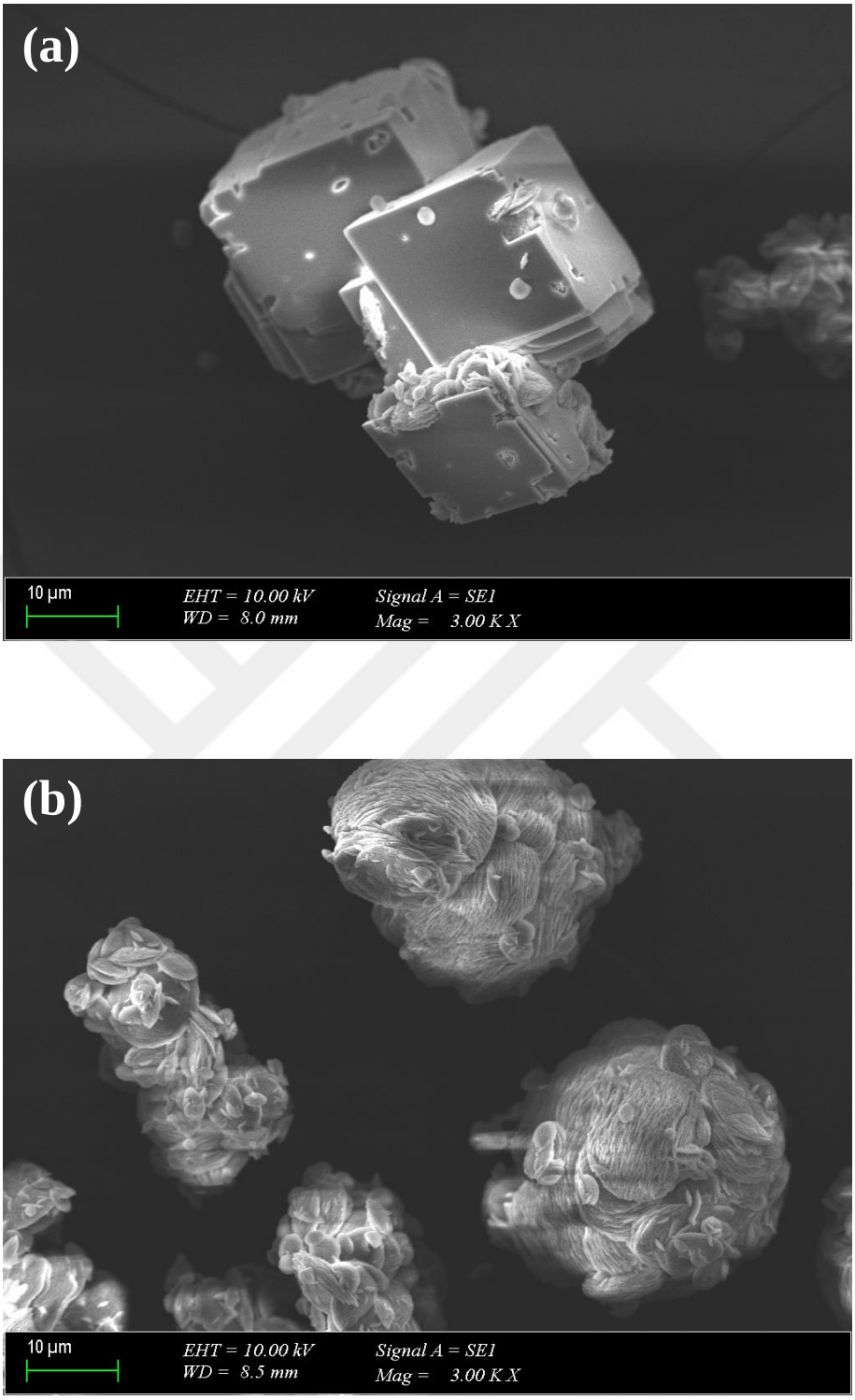

Figure 3.20. SEM images for $CaCO_3$ crystals acquired media supplemented with 50 ppm threonine at t = 30 min (a) and at t = 100 min (b).

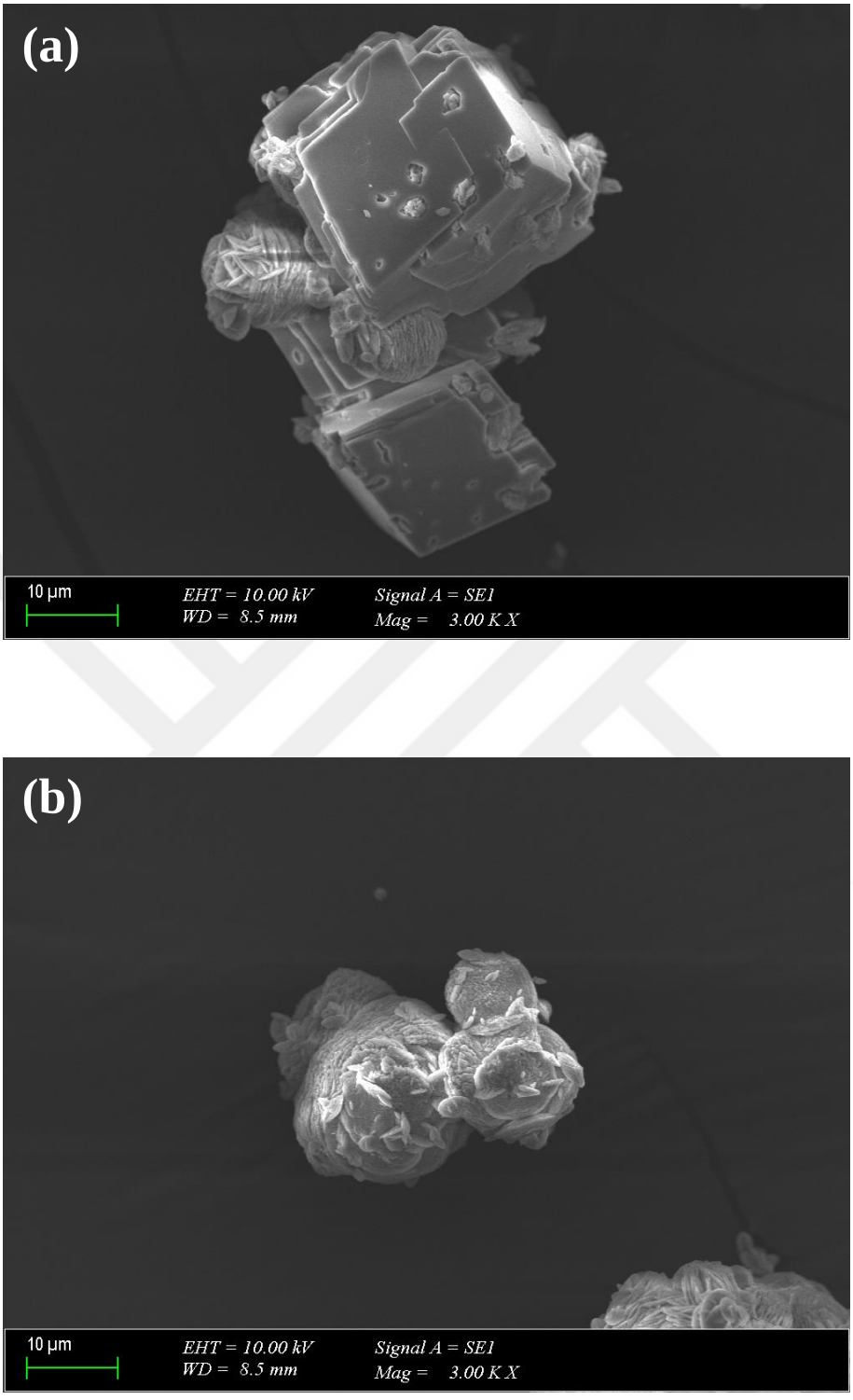

Figure 3.21. SEM images for $CaCO_3$ crystals acquired media supplemented with 100 ppm threonine at t = 30 min (a) and at t = 100 min (b).

3.3.4. Zeta Potential Analysis

Zeta potential analysis was performed to determine the surface charges and stability of the crystals. Figure 3.22 shows the zeta potential analysis results of the $CaCO_3$ crystals precipitated with and without threonine.

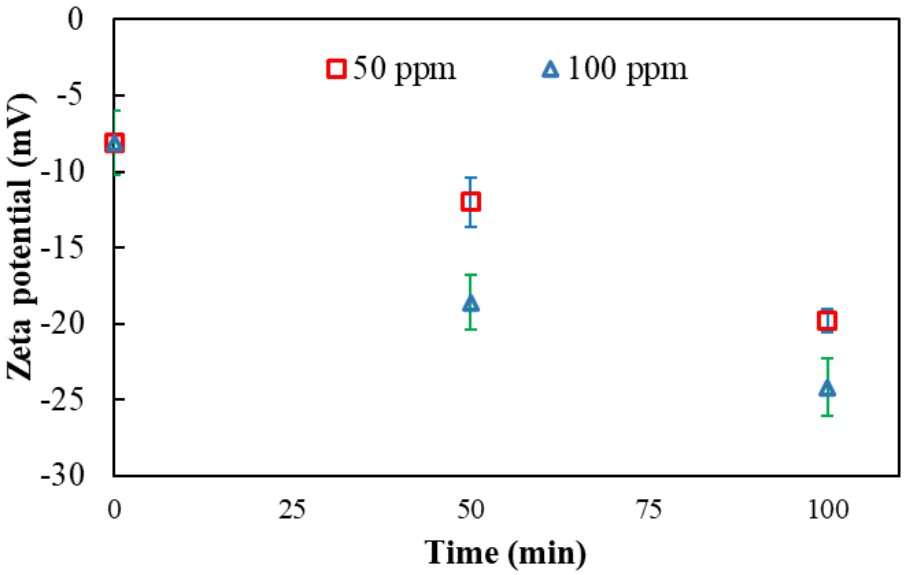

Figure 3.22. The change of zeta potential with time for threonine media.

The surface charge of crystals precipitated in pure media was -8.1 mV. Adding the threonine to the crystallization media made this value even more negative. At the end of the precipitation process, the zeta potential value at 50 and 100 ppm reached –19.8 ± 0.8 and –24.2 ± 1.9 mV, respectively. This result was related to adsorption of the threonine to the crystal surface.

3.3.5. Filtration Analysis

The filtration analysis results for $CaCO_3$ crystals precipitated in threonine media are shown in Table 3.8.

Table 3.8. Filtration analysis results for threonine media.

Media	Concentration (ppm)	Specific cake resistance (m/kg)	Average cake porosity
Pure media	-	1.03×10^{12}	0.548
Threonine media	50	6.04×10^{11}	0.693
	100	2.11×10^{11}	0.747

As seen in Table 3.8, filtration characteristics of $CaCO_3$ crystals were changed due to the change in crystal morphology in additive media. The filtration properties of the crystals precipitated at 50 ppm threonine concentration were improved compared to the pure media. The $CaCO_3$ crystals with less specific cake resistance values were produced in 100 ppm threonine media. As a result, it was found that the threonine had a positive effect on the filtration properties of $CaCO_3$ crystals.

4. CONCLUSION

In this study, the precipitation of $CaCO_3$ was investigated in the presence of different concentrations of tryptophan, glutamic acid, and threonine. Specific conclusions drawn from this work include the following:

- XRD results showed that using 50 ppm tryptophan as an additive increased the vaterite content by 50.0% compared to pure media. In parallel with the XRD results, FTIR analysis demonstrated that the polymorphic transformation from calcite to vaterite was completely achieved in the presence of 100 ppm tryptophan. The XRD and FTIR results showed that although a calcite structure was created in pure media, a vaterite structure was produced in the presence of glutamic acid and threonine.

- SEM images illustrated that tryptophan contributed to the formation of spherical vaterite crystals with a small crystal size. According to the SEM and particle size analysis, the glutamic acid and threonine significantly reduced the size of the crystal and changed its morphology. The mean size of the crystals decreased from 32.0 to 14.6 μm with the use of the glutamic acid additive. It can be suggested that tryptophan, glutamic acid, and threonine could be used as a crystal size and morphology modifiers.

- BET analysis showed that the addition of 100 ppm tryptophan increased the BET specific surface area from 0.7 to 6.4 m^2/g.

- Zeta potential analysis suggested that the tryptophan and threonine tended to adsorb on the crystal surface. The results of the zeta potential measurement suggested that glutamic acid increased the positivity of the surface charge of the $CaCO_3$ crystals.

- Filtration analysis showed that a higher tryptophan, glutamic acid, and threonine concentration led to a higher average cake porosity and a lower specific cake resistance. The values of the average specific cake resistance were calculated in the range of 1.03×10^{12} to 2.11×10^{11} m/kg.

- In this study, the thermal degradation kinetics of $CaCO_3$ were also explored using the Coats–Redfern method. The thermal decomposition kinetics predicted by the R_3 type model showed the best agreement with the experimental data out of the 11 tested

models with high accuracy (R^2 =0.9954). Additionally, this study also provided a thermodynamic analysis of $CaCO_3$ crystals. Based on the R_3 type model, the ΔH, ΔG, and ΔS were calculated to be 215.6 kJ/mol, 297.9 kJ/mol, and −76.0 J/mol K, respectively.

- CCD with RSM was applied successfully to determine how temperature, stirring rate, and tryptophan concentration influenced the $CaCO_3$ polymorphic phase transformation in terms of the amount of vaterite produced. The experimental design results showed that among the investigated factors, additive concentration had the greatest effect on the vaterite content.

- The detailed information about the characterization, kinetics, thermodynamics, and optimization of $CaCO_3$ crystallization obtained in this work will provide a reference for the polymorphic transformation of calcium carbonate for scientific and industrial purposes. It can be concluded that tryptophan, glutamic acid, and threonine are important for better understanding and controlling the polymorph, size, and morphology of $CaCO_3$ crystals.

REFERENCES

[1] Oral, Ç.M., Ercan, B. (2018) Influence of pH on morphology, size and polymorph of room temperature synthesized calcium carbonate particles. Powder Technology, 339, 781-788.

[2] Abeywardena, M.R., Elkaduwe, R.K.W.H.M.K., Karunarathne, D.G.G.P., Pitawala, H.M.T.G.A., Rajapakse, R.M.G., Manipura, A., Mantilaka, M.M.M.G.P.G. (2020) Surfactant assisted synthesis of precipitated calcium carbonate nanoparticles using dolomite: Effect of pH on morphology and particle size. Advanced Powder Technology, 31, 269-278.

[3] Cōlfen, H. (2003) Precipitation of carbonates: recent progress in controlled production of complex shapes. Current Opinion in Colloid & Interface Science, 8, 23-31.

[4] Rodriguez-Blanco, J.D., Shaw, S., Benning, L.G. (2011) The kinetics and mechanisms of amorphous calcium carbonate (ACC) crystallization to calcite, via vaterite. Nanoscale, 3, 265-271.

[5] Zhang, J., Yuzhu, S., Jianguo, Y. (2017) Qualitative discussion of prenucleation cluster role in crystallization of calcium carbonate under high concentration of magnesium based on experimental phenomena. Journal of Crystal Growth, 478, 77-84.

[6] Li, H., Yao, Q., Wang, F., Huang, Y., Fu, S., Zhou, G. (2019) Insights into the formation mechanism of vaterite mediated by a deep-sea bacterium Shewanella piezotolerans WP3. Geochimica et Cosmochimica Acta, 256, 35-48.

[7] Erdogan, N., Eken, H.A. (2017) Precipitated calcium carbonate production, synthesis and properties. Physicochemical Problems of Mineral Processing, 53, 57-68.

[8] Kato, T., Sugawara, A., Hosoda, N. (2002) Calcium Carbonate–Organic Hybrid Materials. Advanced Materials, 14, 869-877.

[9] Saulat, H., Cao, M., Khan, M.M., Khan, M., Khan, M.M., Rehman, A. (2020) Preparation and applications of calcium carbonate whisker with a special focus on construction materials. Construction and Building Materials, 236, 117613.

[10] Fu, L.H., Dong, Y.Y., Ma, M.G., Yue, W., Sun, S.L., Sun, R.C. (2013) Why to synthesize vaterite polymorph of calcium carbonate on the cellulose matrix via sonochemistry process?. Ultrasonics Sonochemistry, 20, 1188-1193.

[11] Carteret, C., Dandeu, A., Moussaoui, S., Muhr, H., Humbert, B., Plasari, E. (2009) Polymorphism Studied by Lattice Phonon Raman Spectroscopy and Statistical Mixture Analysis Method, Application to Calcium Carbonate Polymorphs during Batch Crystallization, Crystal Growth and Design, 9, 807-812.

[12] Kitamura, M. (2002) Controlling factor of polymorphism in crystallization process. Journal of Crystal Growth, 237, 2205-2214.

[13] Flaten, E.M, Seiersten, M., (2009) Polymorphism and morphology of calcium carbonate precipitated in mixed solvents of ethylene glycol and water. Journal of Crystal Growth, 311, 3533-3538.

[14] Hu, Y.B., Wolthers, M., Wolf-Gladrow D.A., Nehrke, G. (2015) Effect of pH and Phosphate on Calcium Carbonate Polymorphs Precipitated at near-Freezing Temperature. Crystal Growth and Design, 15, 1596-1601.

[15] Kim, W.S., Hirasawa, I., Kim, W.S. (2004) Polymorphic Change of Calcium Carbonate during Reaction Crystallization in a Batch Reactor. Industrial & Engineering Chemistry Research, 43, 2650-2657.

[16] Raj, K.S., Devi, N., Subramanian, V.K. (2020) Effect of barium and strontium ions on the morphology and polymorphism of $CaCO_3$. Chemical Physics Letters, 750, 137502.

[17] Yao, Q., Wang, Y., Zhang, Y., Li, H., Zhou, G. (2019) A biomimetic experimental study of magnesium ion mineralization in Mg-enriched aragonite. Science China Earth Sciences, 62, 1619–1629.

[18] Zheng, D., Yang, H., Yu, F., Zhang, B., Cui, H. (2019) Effect of Graphene Oxide on the Crystallization of Calcium Carbonate by C_3S Carbonation. Materials, 12, 2045.

[19] Vidallon, M.L.P., Yu, F., Teo, B.M. (2020) Controlling the Size and Polymorphism of Calcium Carbonate Hybrid Particles Using Natural Biopolymers. Crystal Growth and Design, 20, 645-652.

[20] Kawanoa, M., Maeda, T. (2020) Impact of selenite, arsenate, and silicate oxyanions on the polymorphism and precipitation rate of calcium carbonate minerals in solutions with Mg^{2+} ions. Journal of Crystal Growth, 535, 125536.

[21] Stajner, L., Kontrec, J., Dzakula, B.N., Maltar-Strmecki, N., Plodinec, M., Lyons, D.M., Kralj, D. (2018) The effect of different amino acids on spontaneous precipitation of calcium carbonate polymorphs. Journal of Crystal Growth, 486, 71-81.

[22] Zhao, Z., Zhang, L., Dai, H., Du, Y., Meng, X., Zhang, R., Liu, Y., Deng, J. (2011) Surfactant-assisted solvo-or hydrothermal fabrication and characterization of high-surface-area porous calcium carbonate with multiple morphologies. Microporous and Mesoporous Materials, 138, 191-199.

[23] Butler, M.F., Frith, W.J., Rawlins, C., Weaver, A.C., Heppenstall-Butler, M. (2009) Hollow calcium carbonate microsphere formation in the presence of biopolymers and additives. Crystal Growth and Design, 9, 534-545.

[24] Cölfen, H., Qi, L. (2001) A Systematic Examination of the Morphogenesis of Calcium Carbonate in the Presence of a Double-Hydrophilic Block Copolyme. Chemistry-A European Journal, 7, 106-116.

[25] Sezer, N. (2013) Production of Precipitated Calcium Carbonate From Marble Wastes, Orta Doğu Teknik Üniversitesi Fen Bilimleri Enstitüsü, Doktora Tezi, Ankara.

[26] Chen, Q., Hills, C.D., Yuan, M., Liu, H., Tyrer, M. (2008) Characterization of Carbonated Tricalcium Silicate and its Sorption Capacity for Heavy Metals: A Micron-Scale Composite Adsorbent of Active Silicate Gel and Calcite. Journal of Hazardous Materials, 153, 775–783.

[27] Leeuw, N.H., Parker, S.C. (1998) Surface Structure and Morphology of Calcium Carbonate Polymorphs Calcite, Aragonite, and Vaterite: An Atomistic Approach. The Journal of Physical Chemistry B, 102, 2914-2922.

[28] Koga, N., Kasahara, D., Kimura, T. (2013) Aragonite crystal growth and solid-state aragonite-calcite transformation: A physico-geometrical relationship via thermal dehydration of included water. Crystal Growth and Design, 13, 2238-2246.

[29] Zhang, J., Zhou, X., Dong, C., Sun, Y., Yu, J. (2018) Investigation of amorphous calcium carbonate's formation under high concentration of magnesium: The prenucleation cluster pathway. Journal of Crystal Growth, 494, 8-16.

[30] Trushina, D.B., Bukreeva, T.V., Kovalchuk, M.V. (2014) Antipina MN. $CaCO_3$ vaterite microparticles for biomedical and personal care applications. Materials Science and Engineering: C, 45, 644-658.

[31] Dizaj, S.M., Barzegar-Jalali, M., Zarrintan, M.H., Adibkia, K., Lotfipour, F. (2015) Calcium Carbonate Nanoparticles; Potential in Bone and Tooth Disorders, Pharmaceutical Sciences. 20, 175-182.

[32] Sevcík, R., Sasek, P., Viani A. (2018) Physical and nanomechanical properties of the synthetic anhydrous crystalline $CaCO_3$ polymorphs: vaterite, aragonite and calcite. Journal of Materials Science, 53, 4022–4033.

[33] Aghajanian, S., Koiranen, T. (2020) Dynamic modeling and semibatch reactive crystallization of calcium carbonate through CO_2 capture in highly alkaline water. Journal of CO_2 Utilization, 38, 366-374.

[34] Garg, R.K., Sarkar, D. (2016) Polymorphism control of p-aminobenzoic acid by isothermal anti-solvent crystallization. J. Cryst. Growth, 454, 180-185.

[35] Shi, X., Shao, Y., Sheng X. (2018) A new polymorph of fenofibrate prepared by polymer-mediated crystallization. J. Cryst. Growth, 2018, 498, 93-102.

[36] Jiang, N., Wang, Z., Dang, L., Wei, H. (2016) Effect of supersaturation on L-glutamic acid polymorphs under droplet-based microchannels. J. Cryst. Growth, 446, 68-73.

[37] Strege, C. (2004) On (pseudo-) polymorphic phase transformations, PhD Thesis, Martin-Luther-Universität Halle-Wittenberg, Germany, 1-2.

[38] Braga, D. (2003) Crystal engineering, where from? Where to? Chemical Communications. 2751-2754.

[39] Beckmann, W. (2013) Crystallization Basic Concepts and Industrial Applications, Wiley-VCH Verlag GmbH & Co. KGaA, Germany.

[40] Prohit, R., Venugopalan, P. (2009) Polymorphism: An Overview, Resonance, 14, 882-891.

[41] Agarwal, P. (2002) Calcium Carbonate Crystallization in the Presence of Polymeric Additives, Doctoral Thesis, Michigan State University, A.B.D.

[42] Jones, A.G. (2002) Crystallization Process Systems, Butterworth-Heinemann, London.

[43] Mullin, J. W. (2001) Crystallization, Butterworth-Heinemann, 4th Edition, London.

[44] Ginde, R. M., Myerson, A.S. (1993) Effect of impurities on cluster growth and nucleation, Journal of Crystal Growth, 126, 216-222

[45] Myerson, A.S. (2002) Handbook Industrial Crystallization, 2nd edition Butterworth Heinemann.

[46] Volmer, M. (1939) Kinetic der Phasenbildung, Steinkopff, Leipzig

[47] Mersmann, A. (2001) Crystallization Technology Handbook, Marcel Decker Inc., New York.

[48] Kahana, F., Lehsem, R., Sarig, S. (1995) Selection of Threshold Agents for Calcium Sulfate Scale Control on the Basis of Chemical Structure, Desalination, 17, 215-229.

[49] Koutsoukos, P.G. (1980) Kinetics of Precipitation of Hydroxyapatite from Aqueous Solutions, Doctoral Thesis, State University of New York.

[50] Davey, R.J. (1982) The Role of Additives in Precipitation Processes, Industrial Crystallization, 81, 123-135.

[51] Wade Jr, L.G. (2013) Organic Chemistry, 8th Edition, Prentice Hall, New York.

[52] Bhagavan, N.V., Ha, C.E. (2015) Essentials of Medical Biochemistry, 2nd Edition, Academic Press, 21-29.

[53] Blanco, A., Blanco, G. (2017) Medical Biochemistry, Academic Press, 367-399.

[54] Lehninger, A.L., Nelson, D. L., Cox, M.M. (1993) Principles of Biochemistry, Second Edition, Worth Publishers, Inc USA

[55] Moffett J.R., Namboodiri M.A.A. (2003) Tryptophan and the immune response, Immunology and Cell Biology, 81, 247-265.

[56] Ogunleye A., Bhat A., Irorere V.U., Hill D. (2015) Poly-c-glutamic acid: production, properties and applications. Microbiology 161, 1–17.

[57] Debabov, V.G. (2002) The Threonine Story, Microbial Production of l-Amino Acids, 113-136.

[58] Lin, C.Y., Turchyn, A.V., Steiner, Z., Bots, P., Lampronti, G.I., Tosca, N.J. (2018) The Role of Microbial Sulfate Reduction in Calcium Carbonate Polymorph Selection, Geochimica et Cosmochimica Acta, 237, 184-204.

[59] Siva, T., Muralidharan, S., Sathiyanarayanan, S., Manikandan, E., Jayachandran, M. (2017) Enhanced Polymer Induced Precipitation of Polymorphous in Calcium Carbonate: Calcite Aragonite Vaterite Phases, Journal of Inorganic and Organometallic Polymers and Materials, 27, 770-778.

[60] Sarkar, A., Mahapatra S. (2010), Synthesis of All Crystalline Phases of Anhydrous Calcium Carbonate, Crystal Growth and Design, 10, 2129-2135.

[61] Aquilano, D., Bruno, M., Pastero L. (2020) Impurity Effects on Habit Change and Polymorphic Transitions in the System: Aragonite−Calcite−Vaterite, Crystal Growth and Design, 20, 2497-2507.

[62] Juhasz-Bortuzzo, J.A., Myszka, B., Silva, R., Boccaccini, A.R. (2017) Sonosynthesis of Vaterite-Type Calcium Carbonate, Crystal Growth and Design, 17, 2351-2356.

[63] Yao, C.L., Qı, C.X., Zhu, J.M., Xu, W.H (2010) Unusual Morphology of Calcıum Carbonate Controlled by Amino Acids in Agarose Gel, Journal of the Chilean Chemical Society, 55, 270-273.

[64] Korchef A. (2019) Effect of Iron Ions on the Crystal Growth Kinetics and Microstructure Of Calcium Carbonate, Crystal Growth and Design, 19, 6893-6902.

[65] Lamas, D.G., Neto, M.O., Kellermann G., Craievich, A.F. (2017), Nanocharacterization Techniques, Elsevier, 111–182.

[66] Rajeswari, A., Christy, E.J.S., Gopi, S., Jayaraj K., Pius A. (2020), Interfaces in Particle and Fibre Reinforced Composites, Elsevier, 219-250.

[67] Patel J.P., Parsania P.H. (2018) Biodegradable and Biocompatible Polymer Composites, Elsevier, 55-79.

[68] Kaliva M., Vamvakaki M. (2020) Polymer Science and Nanotechnology, Elsevier, 401-433.

[69] Skoog, D.A., Holler, F.J. ve Nieman, T.A. (1998) Principles of Instrumental Analysis, 5th Edition, Kılıç, E., Köseoğlu, F., Yılmaz, H., (çeviri) Bilim Yayıncılık, Ankara.

[70] Song, K. (2017) Progress in Rubber Nanocomposites, Elsevier, 115-152.

[71] Stuart, B.H. (1997). Biological Applications of Infrared Spectroscopy, John Wiley&Sons Ltd, Chichester.

[72] Ono, D., Bamba, T., Oku, Y., Yonetani T., Fukusaki E. (2011) Application of Fourier transform near-infrared spectroscopy to optimization of gren tea steaming process conditions, Journal of Bioscience and Bioengineering, 112, 247-251.

[73] Lin, S.Y., Wang, S.L. (2012) Advances in simultaneous DSC–FTIR microspectroscopy for rapid solid-state chemical stability studies: Some dipeptide drugs as examples, Advanced Drug Delivery Reviews, 64, 461-478.

[74] Titus D., Samuel E.J.J., Roopan S.M. (2019) Green Synthesis, Characterization and Applications of Nanoparticles, Elsevier, 303-319.

[75] Omidi, M., Fatehinya, A., Farahani, M., Akbari, Z., Shahmoradi, S., Yazdian, F., Tahriri, M., Moharamzadeh, K., Tayebi, L., Vashaee, D. (2017) Biomaterials for Oral and Dental Tissue Engineering, Elsevier, 97-115.

[76] Raval, N., Maheshwari, R., Kalyane, D., Youngren-Ortiz, S.R., Chougule, M.B., Tekade, R.K. (2019) Basic Fundamentals of Drug Delivery, Elsevier, 369-400.

[77] Webb, J, Holgate, J.H. (2003) Encyclopedia of Food Sciences and Nutrition (Second Edition), Elsevier, 3922-3928.

[78] Hameed B.S., Bhatt, C.S., Nagaraj, B., Suresh A.K. (2018) Nanomaterials in Chromatography, Elsevier, 503-518.

[79] Ray, S.S. (2013) Clay-Containing Polymer Nanocomposites, Elsevier, 39-66.

[80] Pentassuglia, S., Agostino, V., Tommasi, T. (2018) Encyclopedia of Interfacial Chemistry, Elsevier,110-123.

[81] Kumar A., Dixit. C.K. (2017) Advances in Nanomedicine for the Delivery of Therapeutic Nucleic Acids, Elsevier, 43-58.

[82] Usui, S., Hachisu, S. (1984) Interaction of Electrical Double Layers and Colloid Stability. In: Electrical Phenomena at Interfaces, Fundamentals, Measurements and Applications, Kitahara, A. and Watanable, A., (Eds.), Marcel Dekker Inc., New York, 47–98.

[83] Fuerstenau, M.C. (1995) Oxide and Silicate Flotation, In: Matis, K.A. (Ed.), Flotation Science and Engineering, Marcel Dekker Inc., New York. 90-126.

[84] Çelik, M.S. and Ersoy, B. (2004) Mineral Nanoparticles: Electrokinetics, Encyclopedia of Nanoscience and Nanotechnology, Ed.: J.A. Schwarz, C.I. Contescu and K. Putyera, Marcel-Dekker Inc, New York.

[85] Asadi, A., Huat, B. B. K., Nahazanan H., Keykhah, H. A. (2013) Theory of electroosmosis in soil, International Journal of Electrochemical Science, 8, 1016-1025.

[86] Hunter, R.J., Foundations of Colloid Science, 2nd Edition. Oxford, England: Oxford University Press (2001).

[87] Saadatkhah, N., Garcia, A.C., Ackermann, S., Leclerc, P., Latifi, M., Samih, S., Patience, G.S., Chaouki, J. (2019) Experimental Methods in Chemical Engineering: Thermogravimetric Analysis-TGA, The Canadian Journal of Chemical Engineering, 98, 34-43.

[88] Tomodaa, B.T., Yassue-Cordeiro, P.H., Ernesto, J.V., Lopes, P.S., Péres, L.O., Silva, C.F., Moraes, M.A. (2020) Biopolymer Membranes and Films, Elsevier, 67-95.

[89] Ebnesajjad, S. (2014) Surface Treatment of Materials for Adhesive Bonding (Second Edition), Elsevier, 39-75.

[90] Choi, K.M., Krudo, K. (2012) Polymorph Control of Calcium Carbonate on the Surface of Mesoporous Silica, Crystal Growth & Design, 12, 887-893.

[91] Liu, Y., Chen, Y., Huang, X., Wu, G. (2017) Biomimetic synthesis of calcium carbonate with different morphologies and polymorphs in the presence of bovine serum albumin and soluble starch, Materials Science and Engineering: C, 79, 457-464.

[92] Bolay, N.L. (2003) On agglomeration phenomena in ball mills: application to the synthesis of composite materials, Powder Technology, 130, 450-455.

[93] Polat, S. (2020) Experimental investigations on the effects of asparagine and serine on the polymorphism of calcium carbonate, Advanced Powder Technology, 31, 4282–4291.

[94] Bastrzyk, A., Fiedot-Tobola, M., Polowczyk, I., Legawiec, K., Plaza, G. (2019), Effect of a lipopeptide biosurfactant on the precipitation of calcium carbonate, Colloids and Surfaces B: Biointerfaces, 174, 145–152.

[95] Kirboga, S., Oner, M., Akyol, E. (2014) The effect of ultrasonication on calcium carbonate crystallization in the presence of biopolymer, Journal of Crystal Growth, 401, 266–270.

[96] Polat, S. (2019) Evaluation of the effects of sodium laurate on calcium carbonate precipitation: Characterization and optimization studies, Journal of Crystal Growth, 508, 8–18.

[97] Popescu, M.A., Isopescu, R., Matei, C., Fagarasan, G., Plesu, V. (2014) Thermal decomposition of calcium carbonate polymorphs precipitated in the presence of ammonia and alkylamines, Advanced Powder Technology, 25, 500-507.

[98] Karunadasa, K.S.P., Manoratne, C.H., Pitawala, H.M.T.G.A., Rajapakse, R.M.G. (2019) Thermal decomposition of calcium carbonate (calcite polymorph) as examined by in-situ high-temperature X-ray powder diffraction, Journal of Physics and Chemistry of Solids, 134, 21-28.

[99] Coats, A.W., Redfern, J.P. (1964) Kinetic Parameters from Thermogravimetric Data, Nature, 201, 68-69.

[100] Mian, I., Li, X., Jian, Y., Dacres, O.D., Zhong, M., Liu, J., Ma, F., Rahman, N. (2019) Kinetic study of biomass pellet pyrolysis by using distributed activation energy model and Coats Redfern methods and their comparison, Bioresource Technology, 294, 122099.

[101] Naqvi, S.R., Tariq, R., Hameed, Z., Ali, I., Naqvi, M., Chen, W.H., Ceylan, S., Rashid, H., Ahmad, J., Taqvi, S.A., Shahbaz, M. (2019) Pyrolysis of high ash sewage sludge: Kinetics and thermodynamic analysis using Coats-Redfern method, Renewable Energy, 131, 854-860.

[102] Kim, Y.S., Kim, Y.S., Kim, S.H. (2010) Investigation of Thermodynamic Parameters in the Thermal Decomposition of Plastic Waste−Waste Lube Oil Compounds, Environmental Science & Technology, 44, 5313-5317.

[103] Fedunik-Hofman, L., Bayon, A., Donne, S.W. (2019) Comparative Kinetic Analysis of $CaCO_3$/CaO Reaction System for Energy Storage and Carbon Capture, Applied Sciences, 9, 4601.

[104] Yue, L., Shui, M., Xu, Z. (1999) The decomposition kinetics of nanocrystalline calcite, Thermochimica, 335, 121-126.

[105] Zheng, T., Zhang, X., Yi, H. (2019) Spherical vaterite microspheres of calcium carbonate synthesized with poly (acrylic acid) and sodium dodecyl benzene sulfonate, Journal of Crystal Growth, 528, 125275.

[106] Wei, Y., Xu, H., Xu, S., Su, H., Sun, R., Huang, D., Zhao, L., Hu, Y., Wang, K., Lian, X. (2020) Synthesis and characterization of calcium carbonate on three kinds of microbial cells template, Journal of Crystal Growth, 547, 125755.

LIST OF PUBLICATIONS ABOUT THE THESIS SUBJECT BEING PREPARED

1. Book Published

1. Sayan P, Polat, S., Ozalp-Şendur, T.N., (2021) Effects Of Amino Acids On Calcium Carbonate Crystallization, LAP LAMBERT Academic Publishing, ISBN:978-620-3-46265-4.

2. Papers Published on Science Citation Expanded Index Journal

1. Polat, S., Ozalp-Şendur, T.N., Sayan P. (2021) Effects of Tryptophan on the Polymorphic Transformation of Calcium Carbonate: Central Composite Design, Characterization, Kinetics, and Thermodynamics, Acta Chimica Slovenica, 68, 414-425.

3. Papers Published on Scopus Index Journal

1. Polat, S., Ozalp, T.N., Sayan P. (2021) Polymorphic Phase Change of Calcium Carbonate with Glutamic Acid as an Additive, Journal of the Turkish Chemical Society Section A: Chemistry, 8(1), 117-124.

4. Presented Announcements

1. T.N. Ozalp, S. Polat, P. Sayan (2020), Optimization of Calcium Carbonate Crystallization in the presence of Threonine Using Response Surface Methodology, International Eurasian Conference on Biotechnology and Biochemistry (BioTechBioChem 2020) (Oral presentation).

2. T.N. Ozalp, S. Polat, P. Sayan (2020), Kinetics Analysis for Calcium Carbonate Prepared using Threonine, International Eurasian Conference on Biotechnology and Biochemistry (BioTechBioChem 2020) (Oral presentation).

3. T.N. Ozalp, S. Polat, P. Sayan (2020), Glutamik Asit Varlığında Kalsiyum Karbonat Kristalizasyonunun İncelenmesi, 32. Online Ulusal Kimya Kongresi. (Oral presentation).

4. T.N. Ozalp, S. Polat, P. Sayan (2020), Kalsiyum Karbonatın Polimorfik Faz Dönüşümünün Ultrasonik Etki Varlığında İncelenmesi, 32. Online Ulusal Kimya Kongresi. (Poster presentation).